HOKKAIDO UNIVERSITY

Title	Study on electroabsorption and electrophotoluminescence of optoelectronic functional materials in solution
Author(s)	姜, 鴻菊
Citation	北海道大学. 博士(環境科学) 甲第11087号
Issue Date	2013-09-25
DOI	10.14943/doctoral.k11087
Doc URL	http://hdl.handle.net/2115/56980
Type	theses (doctoral)
File Information	Chiang_Hung-Chu.pdf

Instructions for use

Hokkaido University Collection of Scholarly and Academic Papers : HUSCAP

Study on Electroabsorption and Electrophotoluminescence of Optoelectronic Functional Materials in Solution

A

Thesis

Presented to the

Hokkaido University

In the fulfillment of the requirement for the Degree of

DOCTOR OF PHILOSOPHY

by

Hung-Chu Chiang

Graduate School of Environmental Science

Hokkaido University

Sapporo, Japan

2013

Contents

Chapter1
Introduction

In photophysical and photochemical research fields, the information about electric properties of molecules associated with the electron transfer of materials is very essential. Interest in determining electrical and optical properties continues to grow, both to understand the fundamental aspects of molecules and molecular aggregates and to design and develop novel functional materials. Electric dipole moment (μ) and molecular polarizability (α) are the most fundamental physical properties. These parameters depend on the state under consideration, and the determination of these parameters at each state is very important not only from the fundamental point from view but also for the point of view of applied science. Stark spectroscopy is a general term describing the study of spectral changes in the presence of electric fields. Depending on μ and α, the state energy is shifted by application of electric field. This spectroscopic technique is useful for probing the electronic and optical responses and the results can be directly related to the difference in the sample's dipole moment ($\Delta\mu$) and polarizability ($\Delta\alpha$) between excited state and ground state. Both parameters contribute significantly to our understanding of electronic structure and electron transfer and related processes of molecules. Moreover, the results of Stark spectroscopy have been used to reassess electron transfer related parameters such as electronic coupling and reorganization energy and the free energy difference [1]. Very recently, it is found that observations in Stark spectroscopy are correlated with the

power conversion efficiency of solar cells in our laboratory. In addition, it has been shown that compounds with large $\Delta\mu$ and $\Delta\alpha$ as well as large transition dipole moment can exhibit large molecular second order nonlinear optical (NLO) properties [2]. Therefore, the quantitative information obtained from Stark spectroscopy are expected to be very helpful in modeling and synthesizing of optoelectronic functional materials in applications such as solar cells, electro-optic modulators, light-emitting diode and chemical sensors, to name just a few.

The terminology, Stark spectroscopy, is based on the Stark effect discovered by Johannes Stark in 1913. Stark observed that splittings of the hydrogen atom Balmer series were induced by application of electric fields. Since then, the field-induced spectral shift has been generally called as the Stark shift on Stark effect. The application of Stark effect to spectroscopy, so-called Stark spectroscopy refers the measurements of field-induced changes in absorption and emission spectra, which are known as electroabsorption (E-A) and electrophotoluminescence (E-PL) spectra, respectively. The spectra can be interpreted in terms of the model developed by Liptay in the 1960s [3], which has played a vital part in describing Stark spectroscopy.

Most studies to date have focused on elucidating the $\Delta\mu$ and $\Delta\alpha$ contribution to the results of E-A and E-PL spectra at films and glasses [4-28], where orientational motion of molecules is literally frozen or suppressed to a great extent. In immobile

phases such as solid films, the electronic response via $\Delta\mu$ and $\Delta\alpha$ is the only dominant contribution, which makes interpretation of the Stark spectra simpler. Further, strong electric field can be applied without any damage of the sample by breakdown, thus permitting precise measurements of electro-optic properties. There are fewer investigations for solution samples. Electronic field effects on absorption and photoluminescence in solution usually show the orientational response to an applied field, and the electric dipole moments of molecule in the ground state and in the emitting state can be obtained.

It has long been interested in quantitatively determining excited state dipole moments. The knowledge of dipole moments in the excited state is not only important in understanding photochemical processes of molecules but also helps to assess the quality obtained from the theoretical approximation methods [3]. Moreover, the orientation induced by electric field of molecules is especially important for optical materials, for example, as optical waveguides [29,30].

Therefore, in the thesis, much effort has been devoted for the development of a measurement system, which enables us to obtain reliable E-A and E-PL spectra of liquid samples. The main goal of this thesis is to utilize an electric field modulation spectroscopy with newly constructed liquid cell and measurement system to study the electric field effect on optoelectronic functional materials in solutions in two aspects:

(1) Electroabsorption spectra were measured in solution to determine the dipole moment, the change in dipole moment, $\Delta\mu$, and change in polarizability, $\Delta\alpha$.

$$\Delta\mu = \mu' - \mu$$
$$\Delta\alpha = \alpha' - \alpha$$

where μ and μ' are the electric dipole moment and α and α' are the polarizability at the ground state and excited state, respectively.

(2) Electrophotoluminescence spectra were measured to examine the electric field effect on the excitation dynamics and to determine the dipole moment at the emitting state.

The organic crystal 4-*N*,*N*-dimethylamino-4'-*N*'-methyl-stilbazolium tosylate (DAST) has been widely studied as a promising candidate for organic NLO materials since DAST takes a noncentrosymmetrically packed crystal structure, due to the Coulombic interactions, which is the basic requirement to provide the second order NLO properties. The high efficiency of the second harmonic generation, which is ca. 1000 times higher than that of urea at 1907 nm, and wideband (0.1−1.5 THz) radiation have rendered the DAST crystal to be a promising material for technological applications such as high speed modulation and frequency mixing applications [31,32]. The recent advances on organic microcrystals, whose sizes are intermediate between a single molecule and bulk crystal, are very attractive for the photonic applications because of their size-dependent unique optical properties. Well-defined

DAST microcrystals can be fabricated by a reprecipitation method, which provides the dispersion liquid of microcrystals, in which organic microcrystals can be easily oriented in a dispersion medium by applying an electric and/or magnetic field. In fact, Fujita et al. [29,30] measured the field-induced absorbance changes of DAST microcrystals by the applied static electric field. The dispersion liquid of microcrystals can be said to have both crystal and liquid properties. The total dipole moment of one DAST microcrystal was estimated to be 2.8×10^7 D in one microcrystal, whose size is $100 \times 100 \times 50$ nm^3, supposing that the dipole moment of one DAST molecule is 30 D [30]. However, the theoretical calculation becomes difficult for large particles.

Pyrene is one of the most well-known compounds that are used so often as a fluorescence probe in material science research and in biological science research because this compound shows strong fluorescence emission, i.e., strong excimer fluorescence, which depends on the distance between two pyrene chromophores and on the polarity surrounding pyrene chromophores [33]. The compound of (carbazole)-$(CH_2)_n$-(terephthalic acid methyl ester), denoted by C-(n)-P, has been widely studied because of the fixed distance of two chromophores and of the through-bond electron transfer between two chromophores [34,35]. In the molecular system in which donor and acceptor are bound to methylene chains, rotations about

the σ-bonds allow the formation of many different conformations in which the intramolecular excited state complex (exciplex) may take place. The E-PL measurements of pyrene and C-(n)-P have been done in polymer solid films [36,37]. The field effects on excimer and exciplex formation processes were observed and have been explained in terms of kinetic models. However, when the samples are doped in polymer solid films, the analysis of the field effects on excitation dynamics is complicated because of the inhomogeneous distribution and the reorientation effect is vanished in the immobile phase. Further, electric field effects on excitation dynamics of chromophores in solution, where chromophores can move easily, may be different from those in solid films, where chromophores are tightly fixed. Then, it is interesting to know how the emission property of pyrene and C-(n)-P is affected by application of an electric field in a mobile system, that is, how the electric field effect on emission characteristics in solution is different from that in solid films.

To address the above mentioned issues, in the present thesis the author employed DAST microcrystal, pyrene, and C-(n)-P compounds to study Stark effects in solutions.

All the measurements are carried out under atmospheric condition. The experimental conditions are described in each chapter. The analysis of the experimental data was done based on theoretical prescription established for Stark

spectroscopy (described in chapter 2). The analysis of the field effects on excitation dynamics of the systems were discussed based on the kinetic model (as will be described in each Chapter).

The present dissertation is arranged as follows:

In chapter 2, optical experimental setup and the design of sample cell are discussed in part 1. The theoretical background of the electric field modulation spectroscopy (Stark spectroscopy) is discussed in part 2.

In chapter 3, the author describes E-A spectra of DAST microcrystal suspension observed with different angles of incidence. The molecular parameters such as dipole moments of ground state were obtained by fitting the Liptay model to the E-A spectra. It is found that experimentally determined dipole moment is much less than theoretical prediction. The electric field effect on absorption spectra of DAST microcrystals as a function of the frequency of the applied electric field is discussed in this chapter.

In chapter 4, the author describes E-A and E-PL spectra of pyrene solution. It is found that the E-A spectra of pyrene in solution are similar in shape to the ones in a polymer matrix. On the other hand, the E-PL measurements show very different results from the ones in solid films. Based on the kinetic analysis, the origin of the

electric field effect on the excimer formation process of pyrene in solution is discussed. A comparison between E-PL spectra of pyrene in solution and in polymer matrix is also discussed in this chapter.

In chapter 5, the author describes the field effect on fluorescence of the series of (carbazole)-$(CH_2)_n$-(terephthalic acid methyl ester) (n = 2-20) in solution. Remarkable field-induced quenching in monomer emission and Stark shift of exciplex were observed. The experimental results are explained in terms of distance-dependent electric field effects on photo-induced electron transfer and exciplex formation. The role of the methylene chain plays in the excitation dynamics of electron transfer and its electric field effect has been discussed in this chapter.

In chapter 6, the author summarized the outcome obtained in each Chapter.

[1] N. Ohta, Electric Field Effects on Photochemical Dynamics in Solid Films. *Bull. Chem. Soc. Jpn*. **2002**, 75, 1637.

[2] K. Yanagi, A. T. Gardiner, R. J. Cogdell, and H. Hashimoto, Electroabsorption spectroscopy of β-carotene homologs: Anomalous enhancement of $\Delta\mu$. *Phys. Rev. B* **2005**, 71, 195118.

[3] W. Liptay, in: E.C. Lim (Ed.), *Excited States*, Academic Press, New York, 1974, p. 129.

[4] N. Ohta, T. Tanaka, I. Yamazaki, A reduction of the high symmetry of C_{60} in a PMMA polymer film as revealed by electroabsorption spectra. *Res. Chem Intermed.* **2001**, *27*, 61-71.

[5] L. L. Premvardhan, L. A. Peteanu, Electronic properties of small model compounds that undergo excited-state intramolecular proton transfer as measured by electroabsorption spectroscopy. *J. Photochem. Photobiol. A Chem*. **2002**, *154*, 69-79.

[6] B. J. Coe, J. A. Harris, B. S. Brunschwig, Electroabsorption Spectroscopic Studies of Dipolar Ruthenium(II) Complexes Possessing Large Quadratic Nonlinear Optical Responses. *J. Phys. Chem. A* **2002**, *106*, 897-905.

[7] A. Chowdhury, L.P. Yu, I. Raheem, L.A. Peteanu, L.A. Liu, D.J. Yaron, Stark Spectroscopy of Size-Selected Helical H-Aggregates of a Cyanine Dye Templated by Duplex DNA. Effect of Exciton Coupling on Electronic Polarizabilities. *J. Phys. Chem. A* **2003**, *107*, 3351-3362.

[8] K. Yanagi, T. Kobayashi, H. Hashimoto, Origin of transition dipole-moment polarizability and hyperpolarizability in hydrazones. *Phys. Rev. B* **2003**, *67*, 115122-115130.

[9] P. R. Bangal, D.M.K. Lam, L.A. Peteanu, M. Van der Auweraer, Excited-State Localization in a 3-Fold-Symmetric Molecule as Probed by Electroabsorption Spectroscopy. *J. Phys. Chem. B* **2004**, *108*, 16834-16840.

[10] W. Stampor, Electroabsorption study of vacuum-evaporated films of Pt(II)octaethylporphyrin. *Chem. Phys*. **2004**, *305*, 77-84.

[9] W. Stampor, J. Mezyk, J. Kalinowski, Electroabsorption study of metal-to-ligand charge transfer in an organic complex of iridium (III). *Chem. Phys.* **2004**, *300*, 189-195.

[11] T. Yoshizawa, Y. Iwaki, N. Osaka, T. Nakabayashi, K.A. Zachariassse, N. Ohta, External Electric Field Effects on Absorption, Fluorescence and Phosphorescence Spectra of 4-(Dimethylamino)benzonitrile in a Polymer Film. *J. Phys. Chem. B*, **2004**, *108*, 19132-19139.

[12] T. Nakabayashi, M. Wahadoszamen, N. Ohta, External Electric Field Effects on State Energy and Photoexcitation Dynamics of Diphenylpolyenes. *J. Am. Chem. Soc*. **2005**, *127*, 7041-7052.

[13] S. Abe, Y. Nishimura, I. Yamazaki, N. Ohta, Remarkable electric field effect on the absorption intensity of a molecular aggregate of photomerocyanine in a PMMA polymer film. *Chem. Lett*. **1999**, 165-166.

[14] N. Kitamura, E. Sakuda, T. Iimori, T. Yoshizawa, N. Ohta, Spectroscopic and Excited-State Properties of Tri-9-anthrylborane II: Electroabsorption and Electrofluorescence Spectra. *J. Phys. Chem. A* **2005**, *109*, 7435-7441.

[15] S. Krawczyk, B. Jazurek, R. Luchowski, D. Wiacek, Electroabsorption spectra of carotenoid isomers: Conformational modulation of polarizability vs. induced dipole moments. *Chem. Phys*. **2006**, *326*, 465-470.

[16] T. M. Smith, N. Hazelton, L. A. Peteanu, J. Wildeman, Electrofluorescence of

MEH-PPV and Its Oligomers: Evidence for Field-Induced Fluorescence Quenching of Single Chains. *J. Phys. Chem. B* **2006**, *110*, 7732-7742.

[17] M. Wahadoszamen, T. Nakabayashi, N. Ohta, Electroabsorption spectra of a complex formed between tetraphenyl-porphyrin and fullerene in a polymer film. *J. Photochem. Photobiol.* **2006**, *178*,177-184.

[18] T. Nakabayashi, B. Wu, T. Morikawa, T. Iimori, M. B. Rubin, S. Speiser, N. Ohta, External electric field effects on absorption and fluorescence of anthracene–(CH_2)n–naphthalene bichromophoric molecules doped in a polymer film. *J. Photochem. Photobiol.* **2006**, *178*, 236-241.

[19] M. S. Mehata, T. Iimori, T. Yoshizawa, N. Ohta, Electroabsorption Spectroscopy of 6-Hydroxyquinoline Doped in Polymer Films: Stark Shifts and Orientational Effects. *J. Phys. Chem. A* **2006**, *110*, 10985-10991.

[20] M.Wahadoszamen, T. Nakabayashi, S. Kang, H. Imahori, N. Ohta, External Electric Field Effects on Absorption and Fluorescence Spectra of a Fullerene Derivative and Its Mixture with Zinc-Tetraphenylporphyrin Doped in a PMMA Film. *J. Phys. Chem. B* **2006**, *110*, 20354-20361.

[21] Y. Ohara, T. Nakabayashi, K. Iwasaki, T. Torimoto, B. Ohtani, T. Hiratanai, K. Konishi, N. Ohta, Electric-Field-Induced Changes in Absorption and Emission Spectra of CdS Nanoparticles Doped in a Polymer Film. *J. Phys. Chem. B* **2006**, *110*, 20927-20936.

[22] N. Ohta, Y. Iwaki, T. Ito, I. Yamazaki, A. Osuka, Photoinduced Charge Transfer along a meso,meso-Linked Porphyrin Array. *J. Phys. Chem*. **1999**, *103*, 11242-11245.

[23] P. A. Lane, H. Mellor, S. J. Martin, T. W. Hagler, A. Bleyer, D. D. C. Bradley, Electroabsorption spectroscopy of distyrylbenzene derivatives. *Chem. Phys.* **2000,** *257*, 41-49.

[24] S. A. Locknar, A. Chowdhury, L. A. Peteanu, Matrix and Temperature Effects on the Electronic Properties of Conjugated Molecules: An Electroabsorption Study of all-trans-Retinal. *J. Phys. Chem. B* **2000**, *104*, 5816-5824.

[25] F. W. Vance, R. V. Slone, C. L. Stern, J. T. Hupp, Comparative absorption, electroabsorption and electrochemical studies of intervalence electron transfer and electronic coupling in cyanide-bridged bimetallic systems: ancillary ligand effects. *Chem. Phys.* **2000**, *253*, 313-322.

[26] B.-C. Chin, K. Misawa, T. Masuda, T. Kobayashi, Large static dipole moment in substituted polyacetylenes obtained by electroabsorption. *Chem. Phys. Lett*. **2000**, *318*, 499-504.

[27] A. Chowdhury, S. Wachsmann-Hogiu, P. R. Bangal, I. Raheem, L. A. Peteanu, Characterization of Chiral H and J Aggregates of Cyanine Dyes Formed by DNA Templating Using Stark and Fluorescence Spectroscopies. *J. Phys. Chem. B* **2001**, *105*, 12196-12201.

[28] L. L. Premvardhan, S. Wachsmann-Hogiu, L. A. Peteanu, D. J. Yaron, P. C. Wang, W. Wang, A. G. MacDiarmid, Conformational effects on optical charge transfer in the emeraldine base form of polyaniline from electroabsorption measurements and semiempirical calculations. *J. Chem. Phys*. **2001**, *115*, 4359-4366.

[29] H. Oikawa, S. Fujita, H. kasai, S. Okada, S. K. Tripathy, and H. Nakanishi, Electric field-induced orientation of organic microcrystals with large dipole moment in dispersion liquid. *Colloids and Surfaces A: Physicochem. and Eng. Aspects* **2000**, *169*, 251-258.

[30] S. Fujita, H. Kasai, S. Okada, H. Oikawa, T. Fukuda, H. Matsuda, S. K. Tripathy, and H. Nakanishi, Electric-field-induced orientation of organic microcrystals with large dipole moment. *Jpn. J. Appl. Phys*. **1999**, *38*, L659-L661.

[31] Seth R. Marder, Joseph W. Perry, William P. Schaefer, Synthesis of Organic Salts with Large Second-Order Optical Nonlinearities. *Science*, **1989**, 245, 626.

[32] U. Meier, M. Bosch, Ch. Bosshard, F. Pan, P. Günter, Parametric interactions in the organic salt 4-N,N-dimethylamino-4'-N'- methyl-stilbazolium tosylate at telecommunication wavelengths. *J. Appl. Phys*. **1998**, *83*, 3486-3489.

[33] Bains, G.; Patel, A. B.; Narayanaswami, V. *Molecules* **2011**, *16*, 7909–7935, and references therein.

[34] F. C. De Schryver, N. Boens, and J. Put, in *Adv. Photochem*., ed by J. N. Pitts, Jr., G. S. Hammond, and K. Gollnick, John Wiley & Sons, New York 1977, Vol. 10, p. 359.

[35] a) P. Pasman, F. Rob, and J. W. Verhoeven, Intramolecular charge-transfer absorption and emission resulting from through-bond interaction in bichromophoric molecules. *J. Am. Chem. Soc*., **1982**, *104*, 5127-5133. b) M. N. Paddon-Row, A. M. Oliver, J. M. Warman, K. J. Smit, M. P. de Haas, H. Oevering, and J. W. Verhoeven, Factors affecting charge separation and recombination in photoexcited rigid donor-insulator-acceptor compounds. *J. Phys. Chem.*, **1988**, *92*, 6958-6962.

[36] N. Ohta, M. Koizumi, S. Umeuchi, Y. Nishimura, and I. Yamazaki, External Electric Field Effects on Fluorescence in an Electron Donor and Acceptor System: Ethylcarbazole and Dimethyl Terephthalate in PMMA Polymer Films. *J. Phys. Chem.* **1996**, 100, 16466.

[37] Ohta, N.; Umeuchi, S.; Kanada, T.; Nishimura, Y.; Yamazaki, I, An enhancement of excimer formation rate of pyrene by an external electric field in a PMMA polymer

film. *Chem*. *Phys*. *Lett*. **1997**, *279*, 215–222.

Chapter 2
Absorption and photoluminescence Stark Spectroscopy

2-1 Experiment

E-A and E-PL spectra were obtained using electric field modulation spectroscopy. The measurements of E-PL and photoluminescence (PL) spectra were preformed by using a fluorescence spectrometer (Jasco, FP777) equipped with a modulation spectrometer apparatus (Fig. 2-1). A Xe lamp was used to provide the light beam in the UV/visible region. The modulated emission signal and transmitted single detected by the photomultiplier tube was extracted and sent to an amplifier (OPA 637) and then ac and dc signals were separated. The dc signal (I) was recorded by an analog-to-digital converter. The ac signal (ΔI) was detected by a lock-in amplifier (SR830, SRS) at the second harmonic frequency (2ω) of the modulation frequency of the applied voltage. Both amplitude and phase of the modulated emission signal detected by the lock-in amplifier were delivered to an analog-to-digital converter. Absorption and E-A spectra in solution were preformed by using a commercially available E-A measurement spectrometer EMV-100, Jasco [1].

The configuration of the cell is schematically shown in Fig. 2-2. The sample was circulated through a sandwich-type cell by using a peristaltic pump. The liquid cell was consisted of two commercially available ITO-coated quartz windows and a polymer spacer. ITO layers were used as the semitransparent electrodes. A silicon-dioxide film was coated on the ITO layer as an insulator film with a thickness

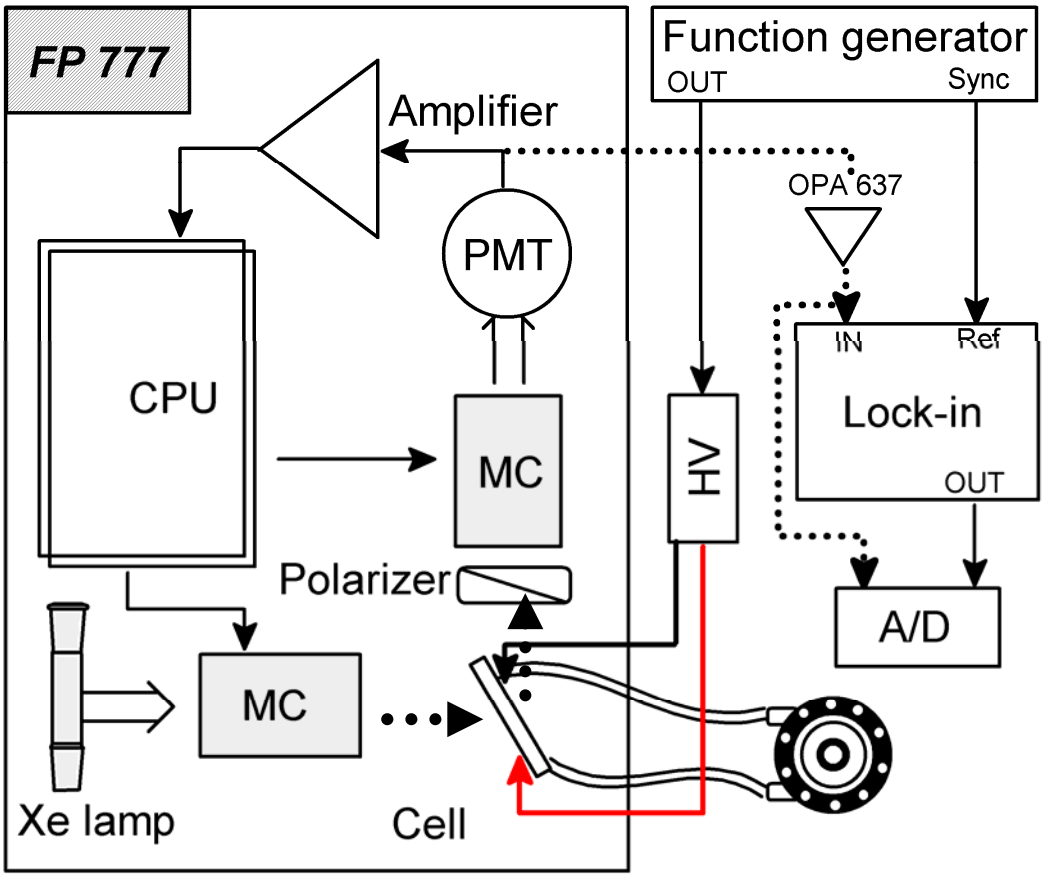

Fig. 2-1 Block diagram of the experimental setup for E-PL measurements. MC: monochromator; HV: High voltage supply; A/D: analog to digital converter.

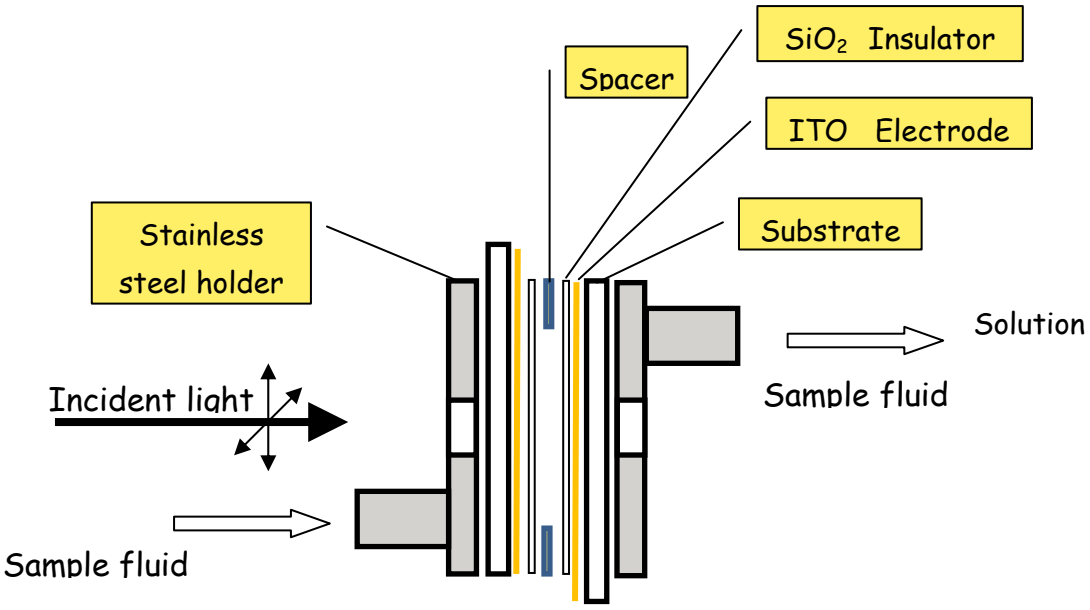

Fig. 2-2 The configuration of the cell

of 0.58 μm. AC voltage was applied to the liquid cell. The strength of the applied electric field was evaluated from the applied voltage divided by the gap between two electrodes of the cell, which was evaluated from interferogram.

2-2 The theoretical background

Stark spectroscopy monitors spectral changes induced by an electric field in absorption and fluorescence spectra of molecules. When an electric field effect is applied to a molecular system, the energy level may be shifted, giving rise to the spectral shift and/or broadening. Therefore, the difference spectrum (field on –field off) is shaped like the first (Stark shift) and second (Stark broadening) derivative of the unperturbed spectrum (field off) as shown in Figs. 2-3,4. Molecular orientation and transition dipole moments (***d***) of a molecule may also be influenced by an electric field, resulting in a change of the spectral intensity as seen in Fig. 2-5.

At first the principle of theoretical basis based on Liptay's theory of Stark spectroscopy is described [2-8]. In the absence of an external electric field, the absorbance at wavenumber $(\bar{\nu})$ is given by

$$\frac{A(\bar{\nu})}{\bar{\nu}} = c\left\langle \Phi_{Ed}^2 \right\rangle s(\bar{\nu}) \tag{1}$$

where $s(\bar{\nu})$ is the band shape function. Φ_{Ed} ($\equiv \cos(\boldsymbol{d} \angle \boldsymbol{E})$) is the cosine of the angle between the transition dipole moment, ***d***, and the polarization direction of the

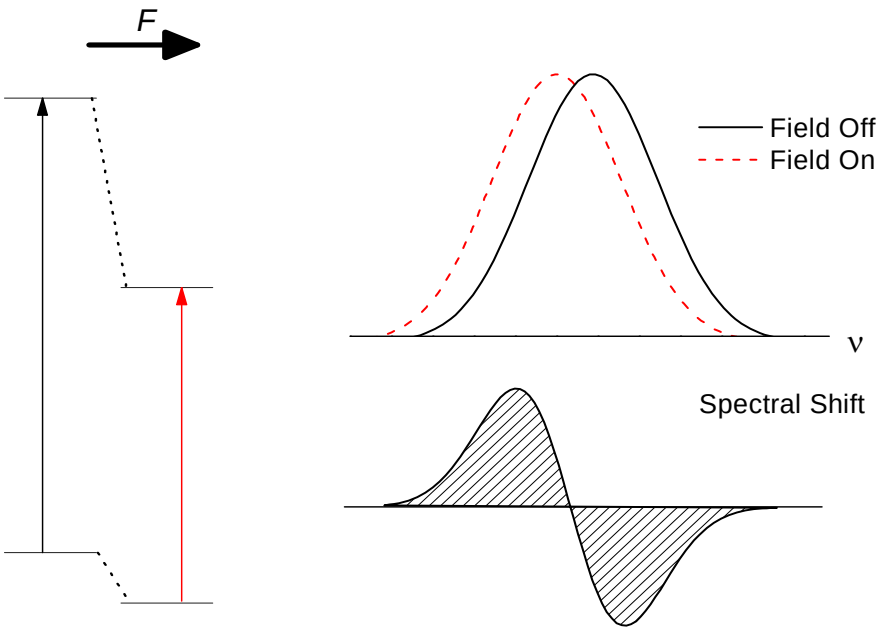

Fig. 2-3 Schematic illustration of the electric effect on spectral lineshape. The difference between the spectra with (dotted line) and without (solid line) an electric field yields the first derivative lineshape.

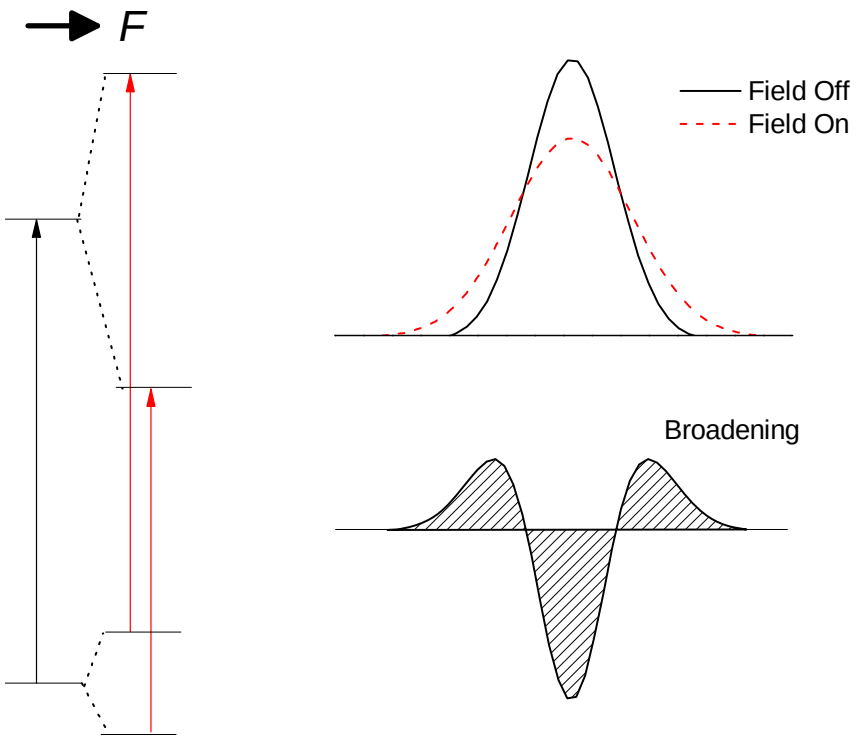

Fig. 2-4 Schematic illustration of the electric effect on spectral lineshape. The difference between the spectra with (dotted line) and without (solid line) an electric field yields the second derivative lineshape.

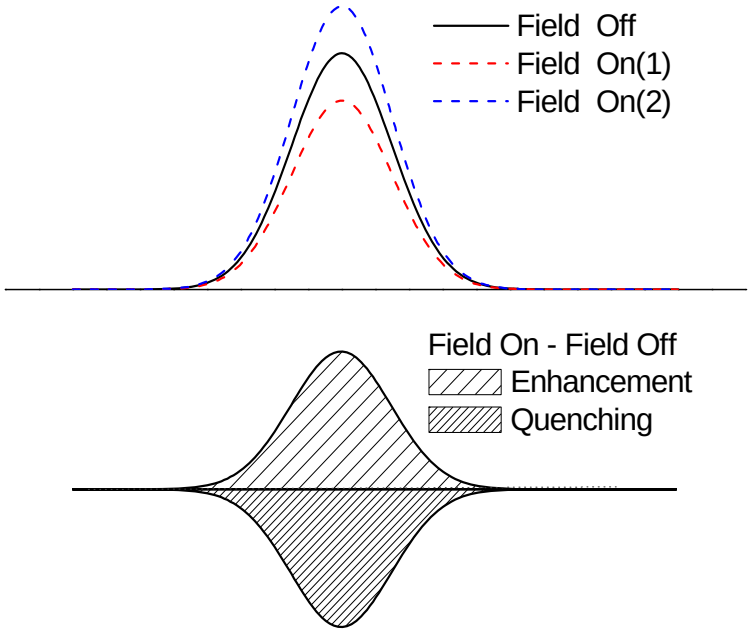

Fig. 2-5 Schematic illustration of the electric effect on spectral lineshape. The difference between the spectra with (dotted line) and without (solid line) an electric field yields a quenching (field on (1) – field off) or an enhancement (field on (2) – field off).

light with the electric field vector, ***E***. The angular brackets, < >, denote the average over all possible orientations of a molecule in an ensemble. $\langle \Phi_{Ed}^2 \rangle$ is 1/3 for an isotropically distributed ensemble. *c* is a constant, which is given by

$$c = \frac{c_a \pi N_A}{\varepsilon_0 h \ln 10} \tag{2}$$

where c_a is the concentration of the absorbing species N_A is Avagadro's number and ε_0 is the electrical permittivity of vacuum, *h* is Planck constant.

When an electric field is applied to the system, absorption could be influenced by an electric field by following reasons (1) field-induced change in band shape function; (2) field-induced reorientation effect.

(1) Field-induced change in band shape function

With a small electric field, it might be reasonable to assume that the absorption band shifts in frequency without any change in band shape. Then the band shape function in the presence of field is related to the same function as the one in the absence of the field by the following equations:

$$s^F(\bar{\nu}) = s(\bar{\nu} - \Delta\bar{\nu}) \tag{3}$$

where $\Delta\bar{\nu}$ represents band shift induced by electric fields. When the Stark shift us very small in comparison with the spectral width of absorption band, the band shape function can be expressed as follows:

$$s^F(\bar{\nu}) = s(\bar{\nu}) - \frac{ds}{d\nu}\Delta\bar{\nu} + \frac{1}{2}\frac{d^2 s}{d\nu^2}(\Delta\bar{\nu})^2 \tag{4}$$

The magnitude of $\Delta\bar{\nu}$ can be obtained as follows:

$$\Delta\bar{\nu} = -\frac{1}{hc}\Delta\mu F\Phi_{F\Delta\mu} - \frac{F^2}{2hc}\sum_{ij}\Phi_{Fi}\Delta\alpha_{ij}\Phi_{Fj} \tag{5}$$

where c is the velocity of light, $\Delta\mu$ the differences in the dipole moment and $\Delta\alpha$ is difference between the molecular polarizability tensor between the excited and ground states. $\Phi_{F\Delta\mu}$ given by $\cos(\boldsymbol{F}\angle\Delta\boldsymbol{\mu})$ is the cosine of the angle between the dipole moment difference and the applied electric field vector, F. The subscripts i and j refer to each component of the vectors or tensors, and the summation is carried out over the x, y and z coordinates.

It is useful to distinguish the shift induced by the interaction between the dipole moment and electric field from the shift induced by the interaction between the polarizability and electric field as follows:

$$\Delta\bar{\nu} = \Delta\overline{\nu_d} + \Delta\overline{\nu_p} \tag{6}$$

where

$$\begin{aligned}\Delta\overline{\nu_d} &= -\frac{1}{hc}\Delta\mu F\Phi_{F\Delta\mu}\\ \Delta\overline{\nu_p} &= -\frac{F^2}{2hc}\sum_{ij}\Phi_{Fi}\Delta\alpha_{ij}\Phi_{Fj}\end{aligned} \tag{7}$$

(2) Field-induced change in orientation

For a thermal ensemble of molecules at temperature T in the presence of electric field, F, the distribution of molecules by energy is given by the Boltzmann formula.

$$w_g^F = \frac{\exp(-E_k^F/kT)}{\langle\exp(-E_k^F/kT\rangle} \tag{8}$$

where E_k^F is the interaction energy of the molecule with the electric field,

$$E_k^F = -\mu F \Phi_{F\Delta\mu} - \frac{F^2}{2}\sum_{ij}\Phi_{Fi}\Delta\alpha_{ij}\Phi_{Fj} \tag{9}$$

Note that the distribution function is defined so that it obeys the normalization condition, i.e., $<w_g>=1$. In the case of the weak electric field, where $\mu F/kT \ll 1$ and $\bar{\alpha}F^2/2kT \ll 1$, the w_g^F can be expressed by their series expansions up to the second order:

$$w_g^F = \frac{1+\frac{\mu F}{kT}\Phi_{F\mu}+\frac{1}{2}\left(\frac{\mu F}{kT}\Phi_{F\mu}\right)^2+\frac{F^2}{2kT}\sum_{ij}\Phi_{Fi}\alpha_{ij}\Phi_{Fj}}{1+\frac{1}{6}\left(\frac{\mu F}{kT}\right)^2+\frac{F^2}{2kT}\bar{\alpha}} \tag{10}$$

where $\bar{\alpha}=\frac{1}{3}\sum_i \alpha_{ii}$ is the average polarizability. For the convenience, the distribution function us approximated as follows:

Using the relation $1/(1+x)\sim 1-x$ with $x \ll 1$.

$$w_g^F = 1 + w_{d1} + w_{d2} + w_p \tag{11}$$

$$w_{d1} = \frac{\mu F}{kT}\Phi_{F\mu} \tag{12}$$

$$w_{d2} = \frac{1}{2}\left(\frac{\mu F}{kT}\Phi_{F\mu}\right)^2 - \frac{1}{6}\left(\frac{\mu F}{kT}\right)^2 \tag{13}$$

$$w_p = \frac{F^2}{2kT}\sum_{ij}\Phi_{Fi}\alpha_{ij}\Phi_{Fj} - \frac{F^2}{2kT}\bar{\alpha} \tag{14}$$

If the indices *i* and *j* in Eq. (14) denote the diagonal components α_{11}, α_{22} and α_{33} ($\alpha_{11}>\alpha_{22}>\alpha_{33}$) of the polarizability tensor, can be written as

$$\sum_{ij}\Phi_{Fi}\alpha_{ij}\Phi_{Fjj} = \bar{\alpha}+\frac{2}{3}\alpha_0\left(\frac{3}{2}\Phi_{F\alpha}^2-\frac{1}{2}\right)+\alpha_x\Psi_{F\alpha}^2\cos 2\Psi' \tag{15}$$

where $\Phi_{F\alpha}$ and $\Psi_{F\alpha}$ are the cosine and sine, respectively, of the angle between the

electric field vector F and the long principal axis of the polarizability tensor and Ψ' is the azimuthal angle about the long principal axis of polarizability tensor between F and the intermediate (second) principal axis of polarizability tensor. The polarizability anisotropy parameters α_0 and α_x are given by

$$\begin{aligned}\alpha_0 &= \alpha_{11} - \frac{1}{2}(\alpha_{22} + \alpha_{33}) \\ \alpha_x &= \frac{1}{2}(\alpha_{22} - \alpha_{33})\end{aligned} \tag{16}$$

Then the field-induced change in absorbance ($\Delta A = A(F) - A(F=0)$) can be expressed in terms of w_g^F and $s^F(\bar{\nu})$.

$$\begin{aligned}\frac{\Delta A}{\bar{\nu}} = \frac{A}{\bar{\nu}} 3 < \Phi_{Ed}^2 w_{d2} > + \frac{d(A/\bar{\nu})}{d\bar{\nu}}(-3) < \Phi_{Ed}^2 \Delta\overline{\nu}_d w_{d1} > + \frac{d^2(A/\bar{\nu})}{d\bar{\nu}^2}\frac{3}{2} < \Phi_{Ed}^2 \Delta\overline{\nu}_d^2 > \\ + \frac{A}{\bar{\nu}} 3 < \Phi_{Ed}^2 w_p > + \frac{d(A/\bar{\nu})}{d\bar{\nu}}(-3) < \Phi_{Ed}^2 \Delta\overline{\nu}_p >\end{aligned} \tag{17}$$

The averages of the products of direction cosines between the axes of two orthogonal Cartesian frames like Φ_{Ed}, $\Phi_{F\mu}$, which consist of the cosine of the angle between laboratory-fixed and molecule-fixed quantities can be expressed by the cosines of the angles between the vectors or between a vector and a tensor axis, both of which belong to the same frame like Φ_{EF}, $\Phi_{d\mu}$ with the direction cosine method [9].

$$\begin{aligned}< \Phi_{Ed}^2 w_{d2} > &= \frac{1}{90}(\frac{\mu F}{kT})^2 (3\Phi_{EF}^2 - 1)(3\Phi_{d\mu}^2 - 1) \\ < \Phi_{Ed}^2 \Delta\overline{\nu}_d w_{d1} > &= -\frac{\mu\Delta\mu F^2}{45hkT}(3\Phi_{EF} - 1)(3\Phi_{d\Delta\mu}\Phi_{d\mu} - \Phi_{\Delta\mu\mu}) + \frac{\mu\Delta\mu F^2}{9hkT}\Phi_{\Delta\mu\mu} \\ < \Phi_{Ed}^2 \Delta\overline{\nu}_d^2 > &= \frac{\Delta\mu^2 F^2}{45h^2}(3\Phi_{EF}^2 - 1)(3\Phi_{d\Delta\mu}^2 - 1) + \frac{\Delta\mu^2 F^2}{9h^2} \\ < \Phi_{Ed}^2 w_p > &= \frac{F^2}{30kT}(3\Phi_{EF}^2 - 1)(\sum_{ij}\Phi_{Fi}\alpha_{ij}\Phi_{Fj} - \bar{\alpha}) \\ < \Phi_{Ed}^2 w_p \Delta\overline{\nu}_p > &= -\frac{F^2}{30kT}(3\Phi_{EF}^2 - 1)(\sum_{ij}\Phi_{Fi}\Delta\alpha_{ij}\Phi_{Fj} - \overline{\Delta\alpha}) + \frac{\overline{\Delta\alpha}F^2}{6h}\end{aligned} \tag{18}$$

As a result, the E-A spectrum can be expressed as the sum of the zeroth, first and

second derivatives of the absorption spectrum as follows:

$$\Delta A(\bar{\nu}) = |f\boldsymbol{F}|^2 \left\{ a_\chi A(\bar{\nu}) + b_\chi \bar{\nu} \frac{\partial}{\partial \bar{\nu}} \left(\frac{A(\bar{\nu})}{\bar{\nu}} \right) + c_\chi \bar{\nu} \frac{\partial^2}{\partial \bar{\nu}^2} \left(\frac{A(\bar{\nu})}{\bar{\nu}} \right) \right\} \tag{19}$$

where f is the internal field factor which relates the magnitude of the field present at the chromophores, F_{int}, to that of the external applied field: $F_{int} = fF_{ext}$. For evaluating f, Lorentz's field correction is usually used: $f = (\varepsilon+2)/3$, where ε is the dielectric constant of the medium. Note that χ represents the angle between the field direction and the polarization direction of the excitation light. a_χ, b_χ and c_χ coefficients can be expressed as follows:

$$\begin{aligned} a_\chi &= \frac{(3\cos^2\chi - 1)}{30kT} \left[\mu^2 (3\cos^2\zeta - 1) + 3(\alpha_m - \bar{\alpha}) \right] \\ b_\chi &= \frac{\mu \Delta\mu \cos\gamma}{3hckT} + \frac{\Delta\bar{\alpha}}{2hc} + \frac{(3\cos^2\chi - 1)}{15hc} \left\{ \frac{\mu\Delta\mu(3\cos\zeta\cos\eta - \cos\gamma)}{kT} + \frac{3(\Delta\alpha_m - \Delta\bar{\alpha})}{2} \right\} \\ c_\chi &= \frac{\Delta\mu^2}{6h^2c^2} + \frac{\Delta\mu^2}{30h^2c^2} (3\cos^2\chi - 1)(3\cos^2\eta - 1) \end{aligned} \tag{20}$$

where μ and $\Delta\mu$ are magnitudes of the ground state dipole moment and the differences in the dipole moment during excitation, respectively. α_m is the polarizability in the ground state with respect to the direction of the transition dipole moment. ζ is the angle between $\boldsymbol{\mu}$ and $\boldsymbol{d}$. γ is the angle between $\boldsymbol{\mu}$ and $\boldsymbol{\Delta\mu}$. η is the angle between $\boldsymbol{\Delta\mu}$ and $\boldsymbol{d}$.

If the transition dipole moment is influenced by an electric field, the field dependence transition dipole moment is given by

$$d^F = d + \sum_i X_{ij} F_i + \frac{1}{2} \sum_{ij} F_i Y_{ijk} F_j + \cdots \tag{21}$$

d is the transition dipole moment vector in the absence of an external electric field. **X** and **Y** are the transition dipole moment polarizability and hyperpolarizability tensors, respectively. Then a_χ and b_χ coefficients are expressed as follows:

$$\begin{aligned} a_\chi &= \frac{1}{3kT|\mathbf{d}|^2} \sum_{ij} (2 d_i X_{ij} \mu_j + X_{ij}^2) + \frac{(3\cos^2\chi - 1)}{30kT} \left[\mu^2 (3\cos^2\zeta - 1) + 3(\alpha_m - \bar{\alpha}) \right] \\ &+ \frac{(3\cos^2\chi - 1)}{15kT|\mathbf{d}|^2} \sum_{ij} (3 d_i X_{ji} \mu_j + 3 d_i X_{jj} \mu_i - 2 d_i X_{ij} \mu_j) + \frac{(3\cos^2\chi - 1)}{15|\mathbf{d}|^2} \sum_{ij} (3 d_i Y_{jij} + 3 d_i Y_{jji} - 2 d_i Y_{ijj}) \\ &+ \frac{1}{30|\mathbf{d}|^2} \sum_{ij} (X_{ij}^2 + (3\cos^2\chi - 1)(3 X_{jj} X_{ii} + 3 X_{ij} X_{ji} + 2 X_{ij})) \end{aligned} \tag{22}$$

$$\begin{aligned} b_\chi &= \frac{\mu \Delta\mu \cos\gamma}{3hckT} + \frac{\Delta\bar{\alpha}}{2hc} + \frac{(3\cos^2\chi - 1)}{15hc} \left\{ \frac{\mu \Delta\mu (3\cos\zeta\cos\eta - \cos\gamma)}{kT} + \frac{3(\Delta\alpha_m - \Delta\bar{\alpha})}{2} \right\} \\ &+ \frac{(3\cos^2\chi - 1)}{15hc|\mathbf{d}|^2} \sum_{ij} (3 d_i X_{ji} \Delta\mu_j + 3 d_i X_{jj} \Delta\mu_i - 2 d_i X_{ij} \Delta\mu_j) + \frac{2}{3hc|\mathbf{d}|^2} \sum_{ij} d_i X_{ij} \Delta\mu_j \end{aligned}$$

The same equations can be applied to emission spectra except that the $\bar{\nu}$-weighting is replaced by $\bar{\nu}^3$-weighting. Here χ is the angle between the external electric field vector and the polarization direction given by an analyzing linear polarizer as shown in Fig. 2-6. The electric field-induced change in fluorescence intensity (ΔI) is expressed as:

$$\Delta I = |f\mathbf{F}|^2 \left\{ a_\chi I + b_\chi \bar{\nu}^{-3} \frac{\partial}{\partial \bar{\nu}} \left(\frac{I}{\bar{\nu}^{-3}} \right) + c_\chi \bar{\nu}^{-3} \frac{\partial^2}{\partial \bar{\nu}^{-2}} \left(\frac{I}{\bar{\nu}^{-3}} \right) \right\} \tag{23}$$

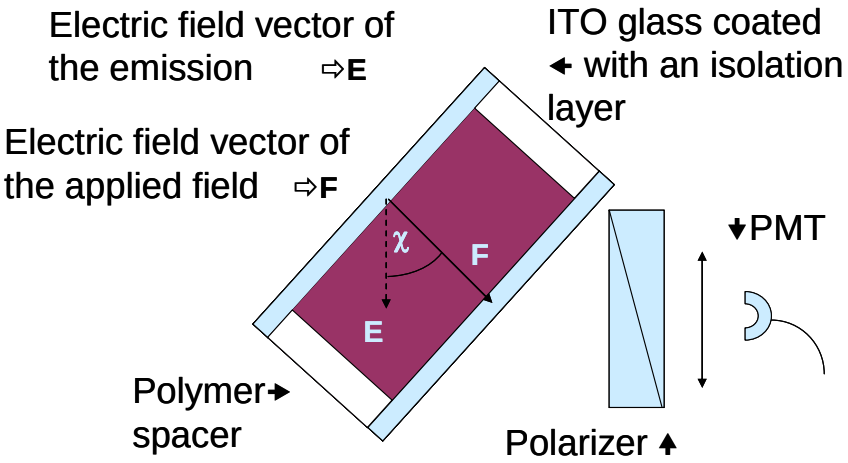

Fig. 2-6 Orientation of the sample slide with respect to the beam for E-PL measurement

[1] Tayama, J.; Iimori, T.; Ohta, N. Comparative Study of Electroabsorption Spectra of Polar and Nonpolar Organic Molecules in Solution and in a Polymer Film. *J. Chem. Phys*. **2009**, *131*, 244509-244509.

[2] E. Jalviste, N. Ohta, Theoretical foundation of electroabsorption spectroscopy: Self-contained derivation of the basic equations with the direction cosine method and the Euler angle method. *J. Photochem. Photobiol. C: Photochem. Rev*. **2007**, *8*, 30-46.

[3] W. Liptay, in: E. C. Lim (Ed.), *Excited states*, Academic Press, New York, 1974, p. 129.

[4] W. Liptay, Electrochromism and Solvatochromism. *Angew. Chem. internat. Edit.* **1969**, *8*, 177-188.

[5] W. Liptay, in: O. Sinanoglu (Ed.), *Modern Quantum Chemistry Part III. Action of Light and Organic Crystals*, Academic Press, New York, 1965, p. 45.

[6] Yamaoka, E. Charney, Electric dichroism studies of macromolecules in solutions. I. Theoretical considerations of electric dichroism and electrochromism. *J. Am. Chem. Soc*. **1972**, *94*, 8963-8974.

[7] Zhou, S.G. Boxer, Probing Excited-State Electron Transfer by Resonance Stark Spectroscopy. 2. Theory and Application. *J. Phys. Chem. B* **1998**, *102*, 9148-9160.

[8] B.Wilson, J.C. Decius, P.C. Cross, *Molecular Vibrations*, McGraw-Hill, New York, **1955**.

Chapter 3
Measurements of electroabsorption spectra of DAST (4-*N*¸*N*-dimethylamino-4-*N*'-methyl -stilbazolium tosylate) microcrystal in solution

3-1 Introduction

The crystal structure of 4-*N*,*N*-dimethylamino-4'-*N*'-methyl-stilbazolium tosylate (DAST) is monoclinic with space-group Cc. The crystallographic parameters are: a = 10.365 Å, b = 11.322 Å, c = 17.893 Å, β = 92.24°; the volume of a crystal cell with 4 molecules was about 2.1 nm^3 [1]. The crystal structure is shown in Fig. 3-1 [2]. The high efficiency of the second harmonic generation, which is ca 1000 times higher than that of urea at 1907 nm, and wideband (0.1-1.5 THz) radiation have rendered DAST crystal to be a promising material for technological applications such as high speed modulation and frequency mixing applications [3-6]. In fact, Fujita et al [7,8] measured the field-induced absorbance changes of DAST microcrystals by applied static electric field, and Kaneko et al. [9] investigated the difference in absorbance with the strength of the applied magnetic field. The linear dependence of relative changes of absorbance on applied fields was observed, owing to microcrystals' orientation. The total dipole moment was estimated to be 2.8×10^7 D in one microcrystal, whose size is 100 × 100 × 50 nm^3, supposing that the dipole moments of one DAST molecule is 30 D [8]. However the theoretical calculation becomes difficult for large particles. The result in this experiment can provide a test for theoretical model Hamilonian to improve the quantitative prediction and the understanding of the polarization property.

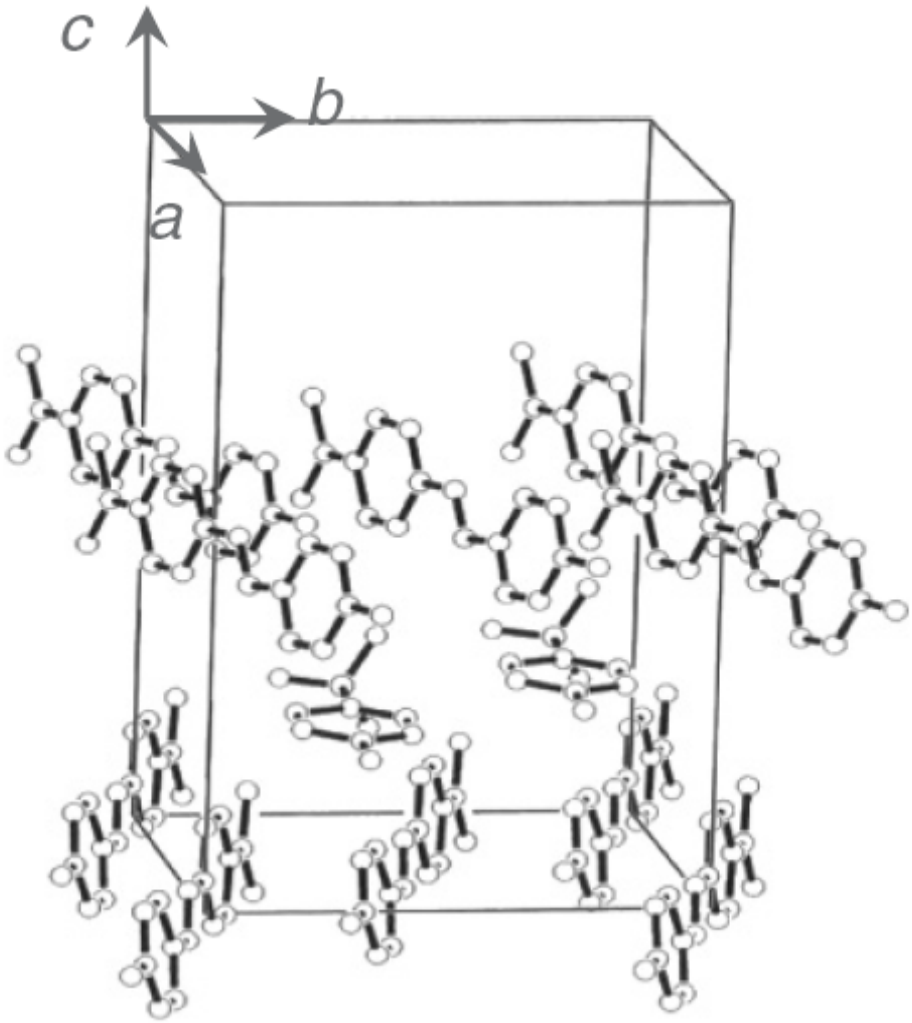

Fig. 3-1 Crystal structure of DAST [2].

3-2 Material

DAST microcrystals were prepared by the reprecipitation method. An amount of 0.5 mL of DAST−ethanol solution (5mM) containing dodecyltrimethylammonium chloride (5 mM) was injected into 50 mL of stirred Acrydic A-1381(surfactant)−decalin solution (0.1 wt %). The chemical structure of constitutes of a DAST crystal and a DAST sample of decalin dispersion liquid are shown below

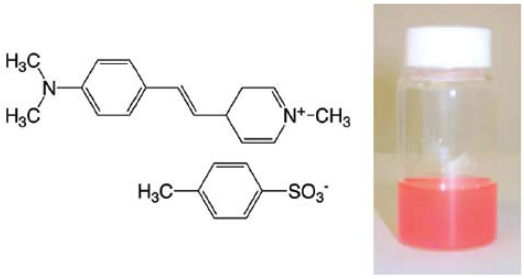

A SEM image (SEM; JSM-6700F, JEOL) of DAST microcrystals filtrated on a filter paper is shown in Fig. 3-2, which shows that DAST microcrystals are rectangular. The coexistence of stabilizer Acrydic A-1381 caused the difficulty in clear observation of SEM images, and so the DLS (DLS; DLS-7000, Ootsuka Electronic Co.) measurements were used to determine the average size of the present DAST crystals. In fact, the crystal size of DAST microcrystals was estimated to be 348 ± 105 nm by the DLS method. Note that DLS is a technique that can be used to determine the size distribution of small particles in suspension or polymers in solution. The size calculated through the Stokes−Einstein equation is the size.

3-3 Results and Discussion

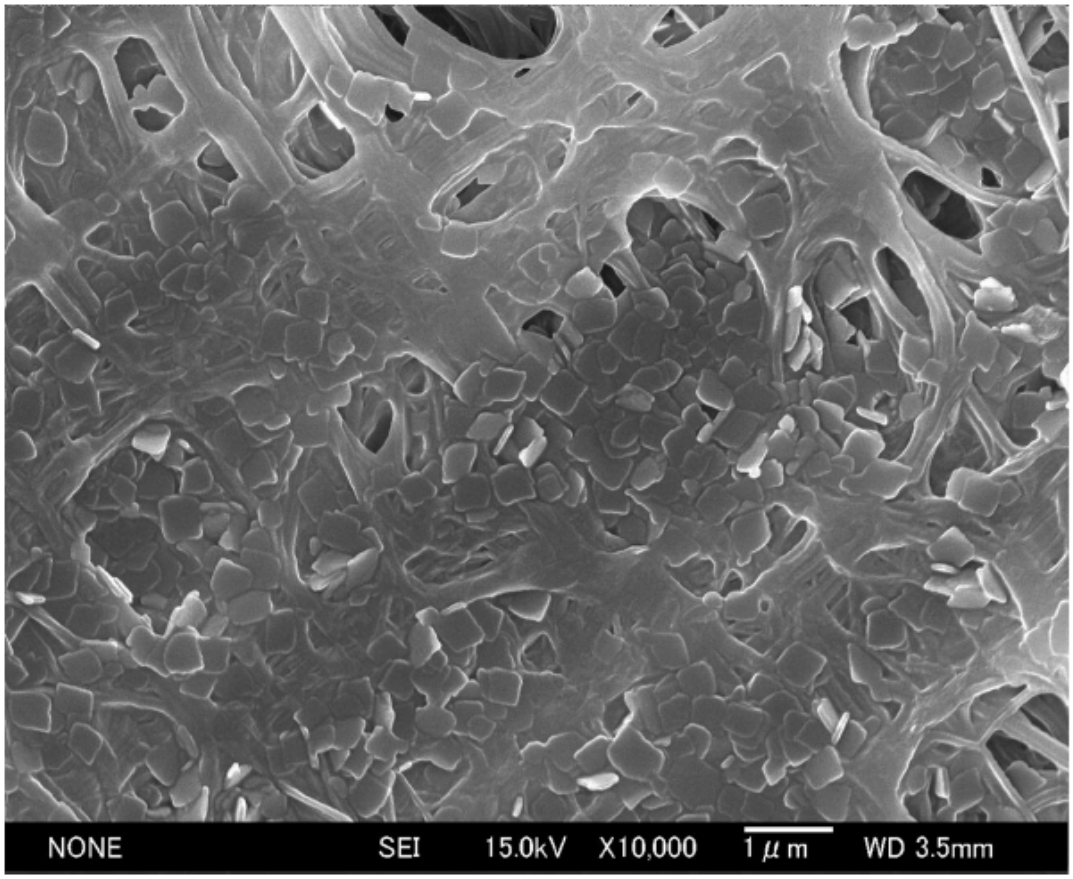

Fig. 3-2 SEM photograph of DAST microcrystals prepared by reprecipitation method.

The absorption spectrum of DAST is shown in Fig. 3-3, where the DAST microcrystals show absorption peak at 553 nm and a shoulder below 500 nm. We also measured the photoluminescence excitation spectrum monitored at 750 nm, which shows a peak at 557 nm and a bandwidth is much narrower than the observed absorption band. Then the observed absorption spectrum is considered to be a superposition of three different bands. By recovering the photoluminescence excitation spectrum, we deconvoluted the absorption band into three components as b1, b2 and b3, as shown in Fig. 3-3. Bhoowmik et al [10] reported the absorption spectrum of a single crystal thin film of DAST, which showed the absorption peak at 550 nm and FWHM ~100 nm (Fig. 3-4). Since both the position and shape of that spectrum are similar to the b2 band, indicating that the b2 is ascribed to a single crystal of DAST, while b1 and b3 might be contributed to different molecular arrangements in DAST microcrystals. Note that the location and shape of the b2 band are the same as the photoluminescence excitation spectrum, and the b1 and b3 bands were obtained by subtracting the b2 band from the total absorption spectrum (see Fig. 3-5). Then the EA spectra are regarded as a sum of the contributions from these three components. $\Delta A = \Delta A^{b1} + \Delta A^{b2} + \Delta A^{b3}$

The observed E-A spectra are shown in Fig. 3-6, together with the absorption spectrum. The E-A spectra remarkably depend on χ. The analysis of the E-A spectra

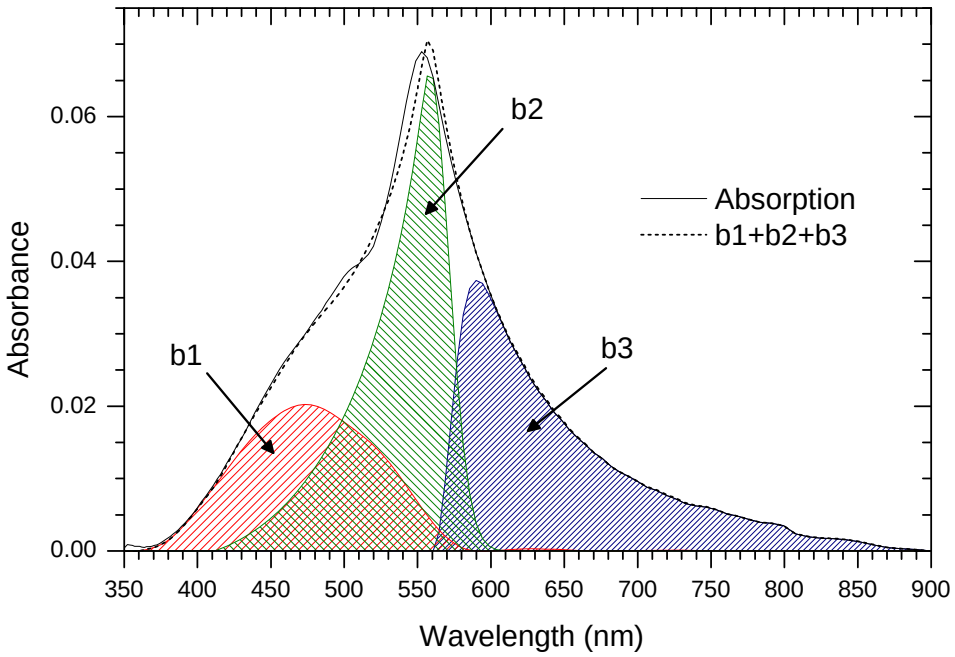

Fig. 3-3 Absorption spectrum of DAST microcrystals in decalin, and the deconvolution of the absorption spectrum into different components

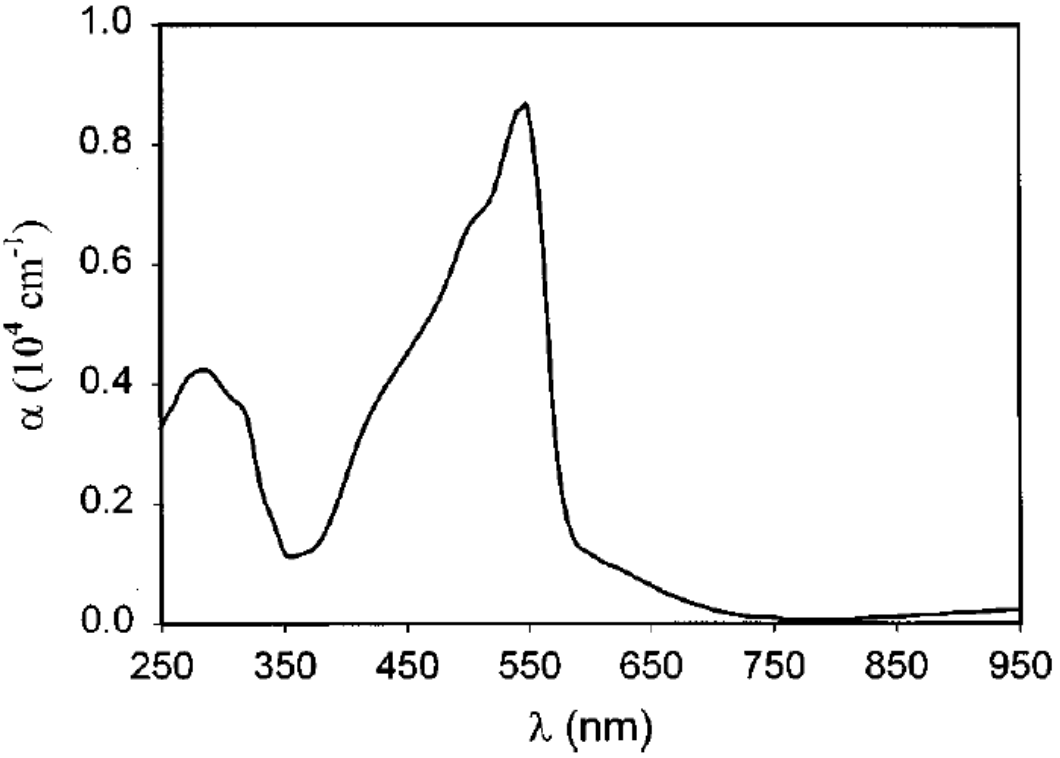

Fig. 3-4 Absorption spectrum of single crystal film of DAST [10]

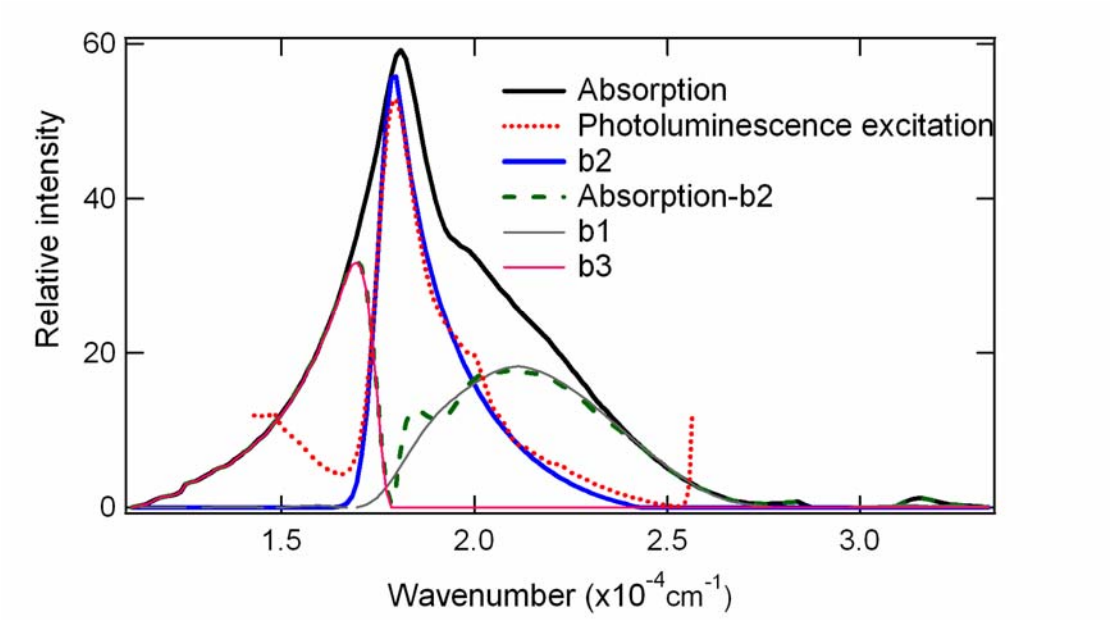

Fig. 3-5 The deconvolution of the absorption spectrum of DAST microcrystals

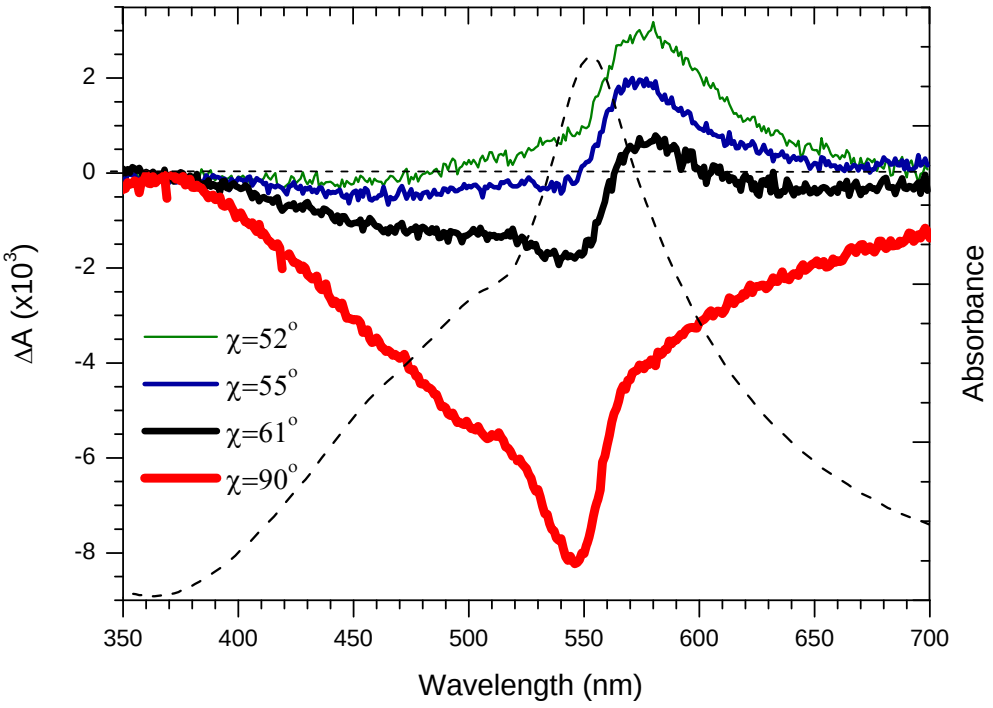

Fig. 3-6 Polarized EA spectra of DAST microcrystals dispersed in decalin observed with different angles of χ. Applied electric filed was 1 kV/cm.

could be done using the decomposed three absorption bands and their derivatives, as shown in Fig. 3-3. In fact, E-A spectra observed at $\chi = 55^{o}$ and $\chi = 90^{o}$ could be well reproduced by a linear combination of the zeroth derivative of b1, b2 and b3 and the first derivative of b2. The non-zero value of the zeroth derivatives at magic angle indicates that the transition dipole moment polarizability is not negligible. It should be noted that the observed E-A spectra couldn't be reproduced by a linear combination of the zeroth, first and second derivatives of the whole absorption spectrum. As a reference, the first derivative of the whole absorption spectrum is shown in Fig. 3-7, in order to show how the E-A spectrum couldn't be reproduced with the derivatives of the whole absorption spectrum.

The contribution of the zeroth derivative is much smaller at $\chi = 55^{o}$ than that at $\chi = 90^{o}$. Then the zeroth derivative component observed at $\chi = 90^{o}$ can be ascribed to the field-induced reorientation, while the zeroth derivative components observed at $\chi = 55^{o}$ is ascribed to the field-induced transition dipole moment polarizability, as mentioned above. The first derivative components can come from field-induced reorientation, the difference in polarizability and/or transition moment polarizability. Actually, in order to achieve the convergence of the fit and to obtain physically meaningful analysis, some assumptions are made that for DAST microcrystals the permanent dipole moment is sufficiently large and the terms related to polarizability

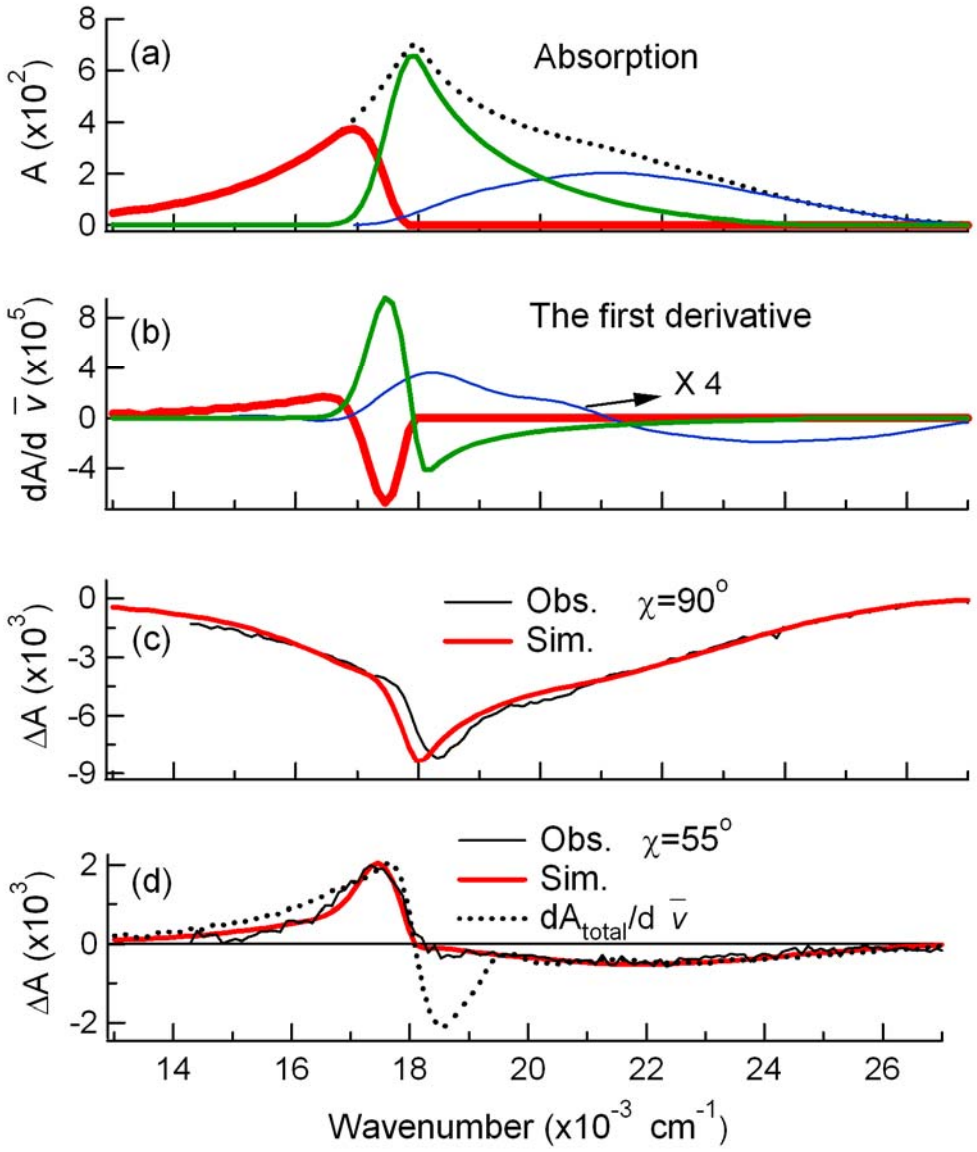

Fig. 3-7 (a). Absorption spectrum and the decomposed absorption bands; together with (b). the first derivative of the decomposed bands; (c). EA spectra of DAST microcrystals observed at $\chi = 90^{o}$ and (d). EA spectra of DAST microcrystals observed at $\chi = 55^{o}$. The first derivative of the whole absorption spectrum (dotted line) is shown in (d). Applied electric filed was 1 kV/cm and 4 Hz.

are negligible in comparison with the terms related to the permanent dipole moment. Further simplification of the molecular angles was done. In space group Cc, the dipole moment of DAST molecule is located in-of-a-c plane of the crystal. The angle between the direction of the dipole moment and a-axis is speculated to be 35^{o}, 4 variable parameters were used in fitting E-A spectra, including A_{χ} for b1, b2 and b3 and B_{χ} for b2. The experimental value of the coefficients used to simulate the observed E-A spectra and the evaluated molecular parameters are listed in Table. 1. In order to examine the response rate of sample to the frequency of *F*, we measured the dependence of ΔT/T on frequency of applied ac voltage. The result is shown in Fig. 3-8. The signal intensity rapidly decreased with an increase in the modulation frequency. By extrapolating the frequency curve to zero, the signal intensity was corrected by the intercept. Field-induced change in absorption intensity thus obtained was used to determine the physical parameters shown in Table 1, though the E-A spectra obtained with a modulation frequency of 4 Hz, as shown in Fig. 3-6. Note the change in frequency of the applied ac voltage doesn't change the shape but the magnitude of the E-A spectrum. As shown in Table 1, the ground state dipole moment is confirmed experimentally to be as large as ~3×10^{4} D for b1, b2 and b3.

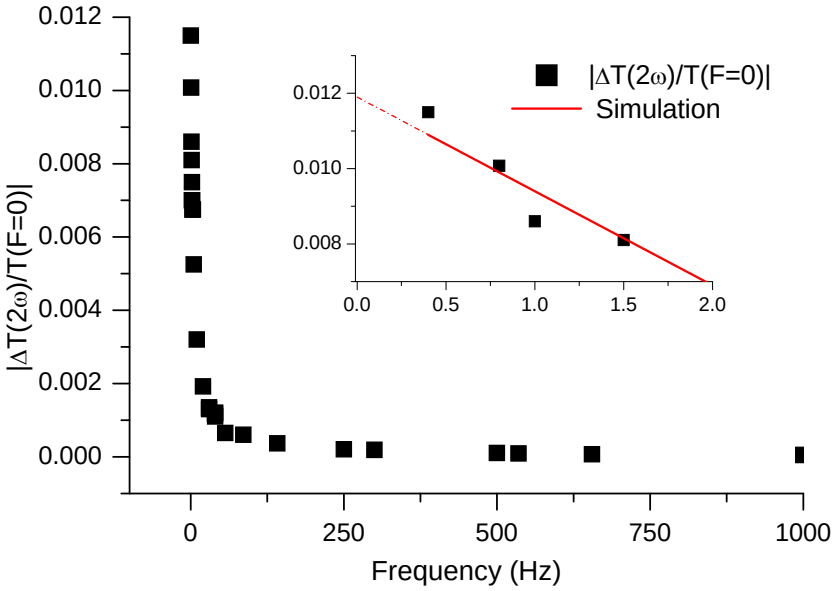

Fig.3-8 The change in transmitted signal related to the transmitted light intensity at zero field as a function of the frequency of the applied electric field. The strength of the applied electric filed was 1 kV/cm.

Table 3-1 Coefficients are used to simulate the E-A spectra and E-A results

	b1	b2	b3
A_{90^o}	-0.17	-0.13	-0.10
B_{90^o}	--	15	--
A_{55^o}	-0.023	0.007	0.020
B_{55^o}	--	15	--
μ ($\zeta = 35^o$)/D	4.8×10^{4}	4.7×10^{4}	4.3×10^{4}
μ ($\zeta = 0^o$) /D	3.4×10^{4}	3.3×10^{4}	3.1×10^{4}
$\Delta\mu$ cos(γ) /D	--	2.5×10^{3}	--
$\sum_{ij}(2d_i X_{ij}\mu_j)/\lvert\mathbf{d}\rvert^2$ /CV-1m^2	-4.9×10^{-32}	1.5×10^{-32}	4.3×10^{-32}

[1] Marder, Joseph W. Perry, William P. Schaefer, Synthesis of Organic Salts with Large Second-Order Optical Nonlinearities. *Science*, **1989**, *245*, 626-628.

[2] T. Matsukawa, M. Yoshimura, Y. Takahashi, Y. Takemoto, K. Takeya, I. Kawayama, S. Okada, M. Tonouchi, Y. Kitaoka, Y. Mori, and T. Sasaki, Bulk Crystal Growth of Stilbazolium Derivatives for Terahertz Waves Generation. *Jpn. J. Appl. Phys*.**2010**, *49*(7), 075502-075507.

[3] U. Meier, M. Bosch, Ch. Bosshard, F. Pan, P. Günter, Parametric interactions in the organic salt 4-N,N-dimethylamino-4'-N'- methyl-stilbazolium tosylate at telecommunication wavelengths. *J. Appl. Phys*. **1998**, *83*, 3486-3489.

[4] T. Taniuchi, S. Okada, and H. Nakanishi, Widely-tunable THz-wave generation in 2–20 THz range from DAST crystal by nonlinear difference frequency mixing. *Electron. Lett*. **2004**, *40*, 60-62.

[5] F. Pan, K. McCallion, M. Chiapppetta, Waveguide fabrication and high-speed in-line intensity modulation in 4-*N*,*N*-4'-dimethylamino-4'-*N*'-methyl-stilbazolium tosylate. *Appl. Phys. Lett.* **1999**, *74*, 492-494.

[6] P. Y. Han, M. Tani, F. Pan, X. C. Zhang, Use of the organic crystal DAST for terahertz beam applications. *Opt. Lett*. **2000**, *25*, 675-677.

[7] S. Fujita, H. Kasai, S. Okada, H. Oikawa, T. Fukuda, H. Matsuda, S. K. Tripathy, and H. Nakanishi, Electric-field-induced orientation of organic microcrystals with large dipole moment. *Jpn. J. Appl. Phys*. **1999**, *38*, L659-L661.

[8] H. Oikawa, S. Fujita, H. kasai, S. Okada, S. K. Tripathy, and H. Nakanishi, Electric field-induced orientation of organic microcrystals with large dipole moment in dispersion liquid. *Colloids and Surfaces A: Physicochem. and Eng. Aspects* **2000**, *169*, 251-258.

[9] Y. Kaneko, S. Shimada, T. Fukuda, T. Kimura, H. Yokoi, H. Matsuda, T. Onodera,

H. Kasai, S. Okada, H. Oikawa, and H. Nakanishi, A novel method for fixing the anisotropic orientation of dispersed organic nanocrystals in a magnetic field. *Adv. Mater*.**2005**, *17*, 160-163.

[10] A. K. Bhowmik, J. Xu, and M. Thakur, Polarized optical absorption and photoluminescence measurements in single-crystal thin films of 4'-dimethylamino-N-methyl-4-stilbazolium tosylate. *Appl. Phys. Lett.* **1999**, *75*, 3291-3293.

Chapter 4
Electric field effect on fluorescence and excitation dynamics of pyrene in solution

4-1 Introduction

As reported in our previous papers [1-2] electric field effects on fluorescence of pyrene have been examined in a solid film of poly(methyl methacrylate) (PMMA), where pyrene showed three kinds of emissions at high concentrations, i.e., monomer fluorescence emitted from the locally excited state of pyrene, sandwich-type excimer fluorescence, and partially overlapped second excimer fluorescence. It was found that monomer fluorescence and sandwich-type excimer fluorescence are quenched by application of electric fields, whereas second excimer fluorescence is enhanced by electric fields. Based on the results, excitation dynamics of this compound in the presence of electric field was discussed. As far as experiments are performed in solid films, the mobility of molecules is limited, though the observed electric field effect on fluorescence reflects the inhomogeneous distribution of pyrene molecules. For example, the second excimer, whose fluorescence was confirmed in the electric field effects on photoluminescence in a PMMA film, probably results from immobility of molecules in a solid matrix because this species seems to be much less stable than the sandwich type excimer.

Many experiments have been done using pyrene and its derivatives as a fluorescence probe in biological system [3-5]. Since charged and polar groups within protein structures produce a strong electric field for embedded molecules emission

property as well as dynamics of chromophores located in biological system may be significantly affected by such a strong electric field. Further, electric field effects on dynamics of chromophores in biological system and in solution, where chromophore can move easily, may be different from that in solid films where chromophores are tightly fixed. Then it is interesting to know how emission property of pyrene is affected by application of electric field in mobile system, that is, how the electric field effect on emission characteristics in solution is different from that in solid films.

In the present study we have measured E-PL spectra of pyrene in solution, along with the E-A spectra. The experimental results are explained in terms of a kinetic model which is used to explain the emission property of pyrene in solution.

4-2 Material

Pyrene solution was prepared with a mixture of benzene and decalin as a solvent. Pyrene and decalin (Kanto Chem.) and benzene dehydrated (Wako Chem.) were used without further purification. Pyrene crystal was dissolved in 2 ml benzene, which was stirred and then diluted into 10 ml decalin. The binary non-polar solvent was employed because of the high thermal stability and solubility. AC voltage (4 kHz) was applied to the liquid cell.

4-3 Results and Discussions

Absorption intensity (A) and E-A signal (ΔA) of pyrene solution with a

concentration of 5 x 10^{-2} M were obtained for the S_2-S_0 absorption region. Both absorption and E-A spectra are shown in Fig. 4-1, together with the first derivative spectrum of the absorption spectrum. E-A spectrum of pyrene obtained with a field strength of 0.1 $MVcm^{-1}$, as is shown in Fig.4-1. (b) is essentially the same as the first derivative of the absorption spectrum, indicating that the E-A signal comes from the change in polarizability between the ground state and the absorption state, as already reported [6].

Fig. 4-2 shows the E-PL spectrum of pyrene in solution at 5 x 10^{-3} M, together with the PL spectrum simultaneously observed with a spectral resolution of 10 nm. The E-PL spectrum was obtained with a field strength of 0.2 $MVcm^{-1}$ with excitation at 30770 cm^{-1}, where the field-induced change in absorbance is negligibly small.

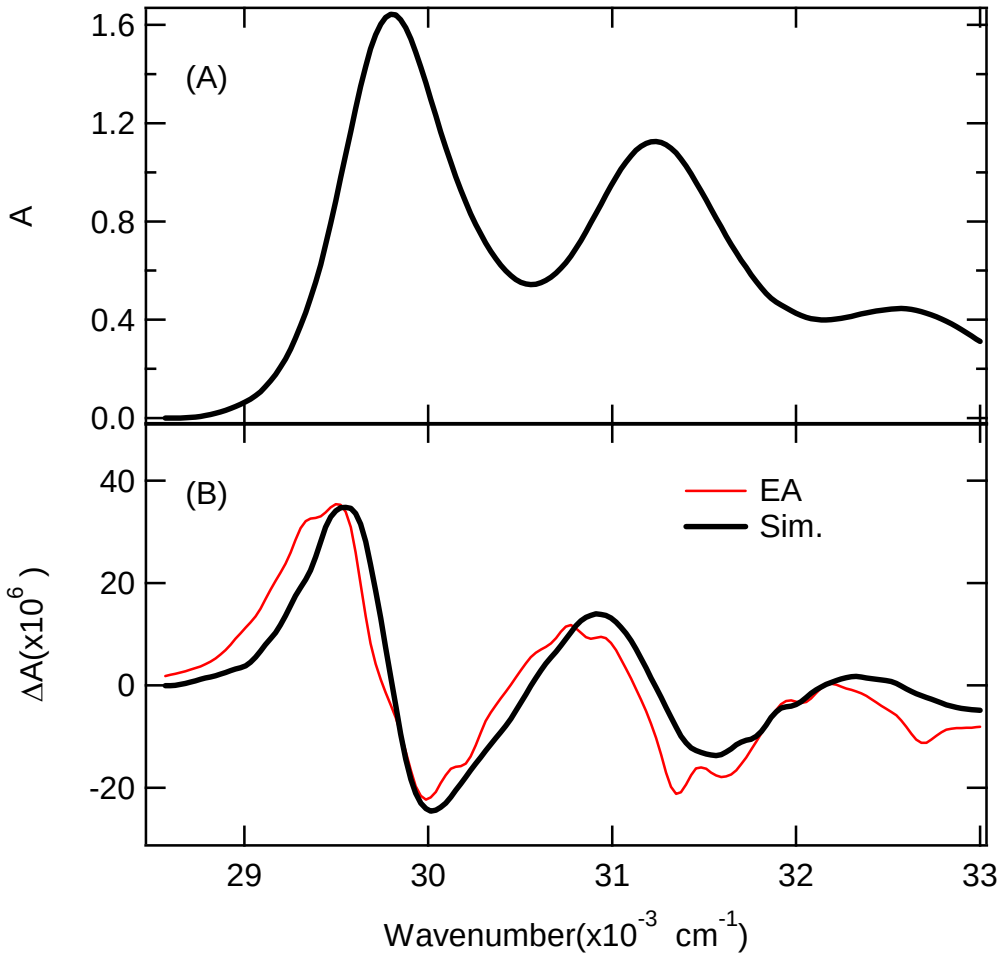

Fig. 4-1. (A) Absorption spectrum of pyrene solution at a concentration of 0.05 M, (B) the first derivative spectrum of the above absorption spectrum and E-A spectrum observed with a field strength 0.1 MVcm^{-1}.

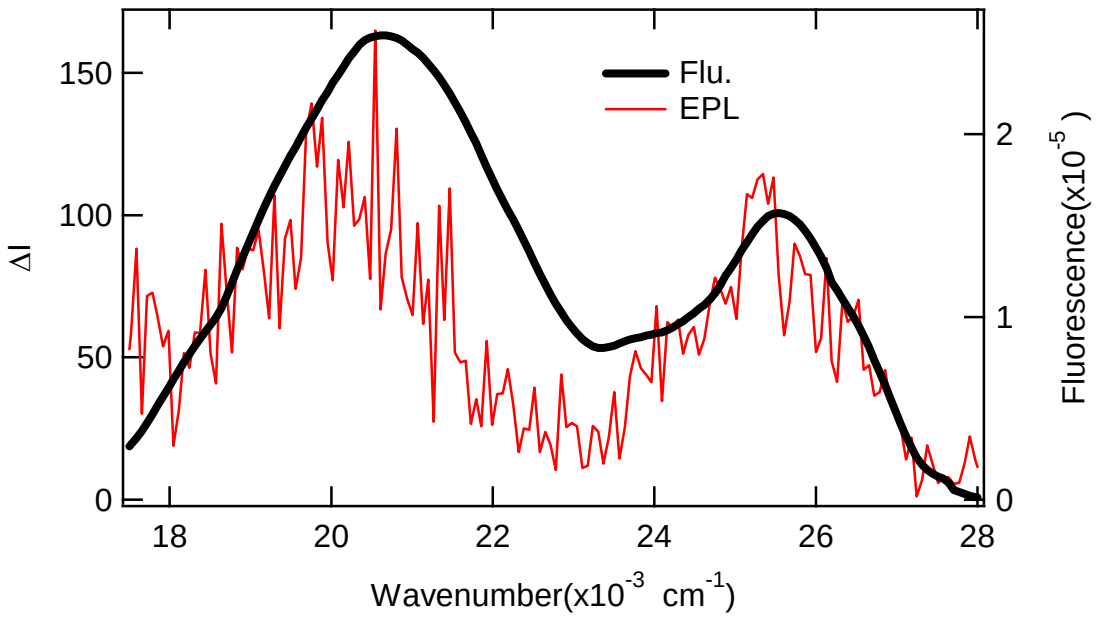

Fig. 4-2. Emission spectrum and E-PL spectrum of pyrene solution 5 x 10^{-3} M. Excitation wavenumber was 30770 cm^{-1}. Applied field strength was 0.2 $MVcm^{-1}$.

$\Delta I_{PL}(\bar{\nu})/I_{PL}(\bar{\nu})$ at 25800 cm^{-1}, which corresponds to the peak position of the monomer fluorescence spectrum, as described below, was obtained as a function of the square of the applied electric field strength (see Fig. 4-3). Note that $I_{PL}(\bar{\nu})$ and $\Delta I_{PL}(\bar{\nu})$ represent PL intensity and its field-induced change at wavenumber of $\bar{\nu}$, respectively. As shown in Fig. 4-3, the field-induced change in fluorescence intensity is proportional to the square of the applied electric field strength.

PL spectrum of pyrene solution at high concentrations shows two emissions, i.e., monomer fluorescence emitted from the locally excited state of pyrene and sandwich-type excimer fluorescence, which show the peak at 25800 cm^{-1} and at 20880 cm^{-1}, respectively, in the present spectral resolution. As shown in Fig. 4-2, both emissions are enhanced by application of electric fields at a concentration of 5 x 10^{-3} M, and the magnitude of the field-induced enhancement relative to the total PL intensity is larger in monomer fluorescence than the other. The second excimer fluorescence, which shows a peak at 415 nm (24096 cm^{-1}) and whose intensity is enhanced by $\boldsymbol{F}$ in a PMMA film [6], was not confirmed in solution both in PL spectrum and in E-PL spectrum. In addition to the field-induced change in intensity, the sandwich-type excimer fluorescence is red-shifted with $\boldsymbol{F}$, as shown in Fig. 4-2. As a result, the E-PL spectrum of pyrene solution could be simulated by a linear combination of the zeroth derivative of each of the monomer and excimer

fluorescence spectra and the first derivative of the excimer fluorescence spectrum, as follows:

$$\Delta I_{PL}(\bar{\nu}) = (f\boldsymbol{F})^2 \left[aI_M(\bar{\nu}) + bI_D(\bar{\nu}) + c\bar{\nu}^3 \left[\mathrm{d}\left\{ I_D(\bar{\nu})/\bar{\nu}^3 \right\} / \mathrm{d}\bar{\nu} \right] \right] \quad (1)$$

where f is the internal field factor, and $I_M(\bar{\nu})$ and $I_D(\bar{\nu})$ are monomer fluorescence intensity and excimer fluorescence intensity, respectively, at wavenumber of $\bar{\nu}$. a, b and c are coefficients. The first and second terms correspond to the field-induced change in fluorescence intensity, while the third term arises from the difference in polarizability between the emitting state of excimer and the ground state of monomer.

As shown in Fig. 4-4, the monomer and excimer bands are decomposed by assuming that the spectral shape both of the monomer fluorescence and of the excimer fluorescence is independent of the concentration of pyrene. Based on the evaluation of the first derivative component in the E-PL spectrum of the excimer fluorescence, the value of the change in molecular polarizability following the excimer emission, i.e., $f^2\Delta\bar{\alpha}$, was determined to be ~270±90 Å^3 for excimer, which is much larger than that obtained for monomer fluorescence in a PMMA film. Note that the magnitude of $f^2\Delta\bar{\alpha}$ of monomer fluorescence was reported to be ~ 15 Å^3 in a PMMA film [6].

E-PL spectra were also obtained at different concentrations of 7 x 10^{-4} and 3 x 10^{-3} M with a field strength of 0.2 MVcm^{-1}. The results are shown in Fig. 4-5. Signal to

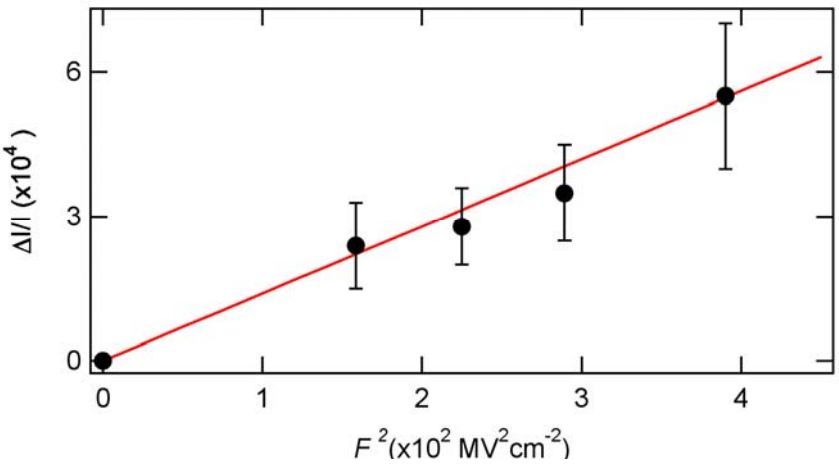

Fig. 4-3. Plots of the field-induced change in monomer emission intensity relative to its fluorescence intensity as a function of the square of the applied electric field

noise ratio is very low, but it is confirmed that monomer fluorescence is enhanced by application of electric fields at these concentrations. It should be also noted that excimer fluorescence at a concentration of 3 x 10^{-3} M is also enhanced by ***F*** and that the magnitude of the enhancement relative to the fluorescence intensity for excimer is smaller than that of monomer, in agreement with the results at 5 x 10^{-3} M shown in Fig. 4-2.

E-PL spectra show that monomer fluorescence and excimer fluorescence give different field dependence of quantum yield from each other. The following kinetic model is usually applied to interpret the excimer formation of pyrene in solution [8].

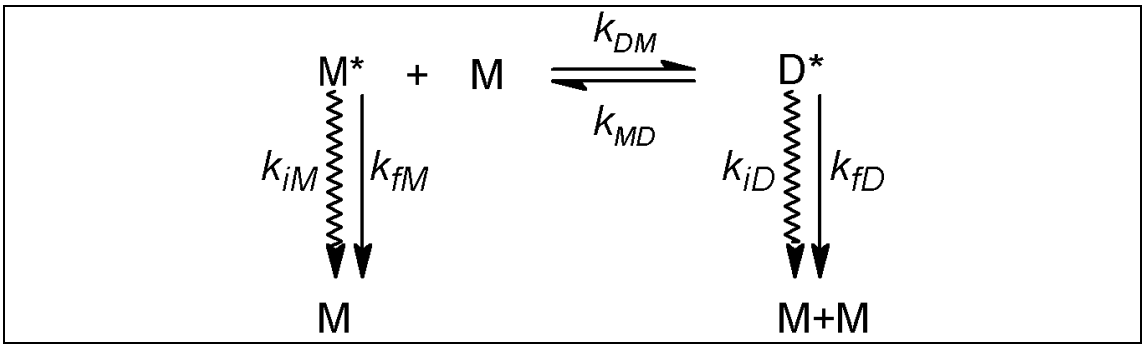

Here, M is the ground state monomer; M* and D* are the excited monomer and excimer, which give monomer fluorescence and excimer fluorescence, respectively; k_{DM} and k_{MD} are the rate constants of excimer formation and dissociation of D* to M* and M, respectively; k_{fM} and k_{fD} are the radiative rate constant of M* and D*, respectively; k_{iM} and k_{iD} are the nonradiative rate constant of M* and D*, respectively

.

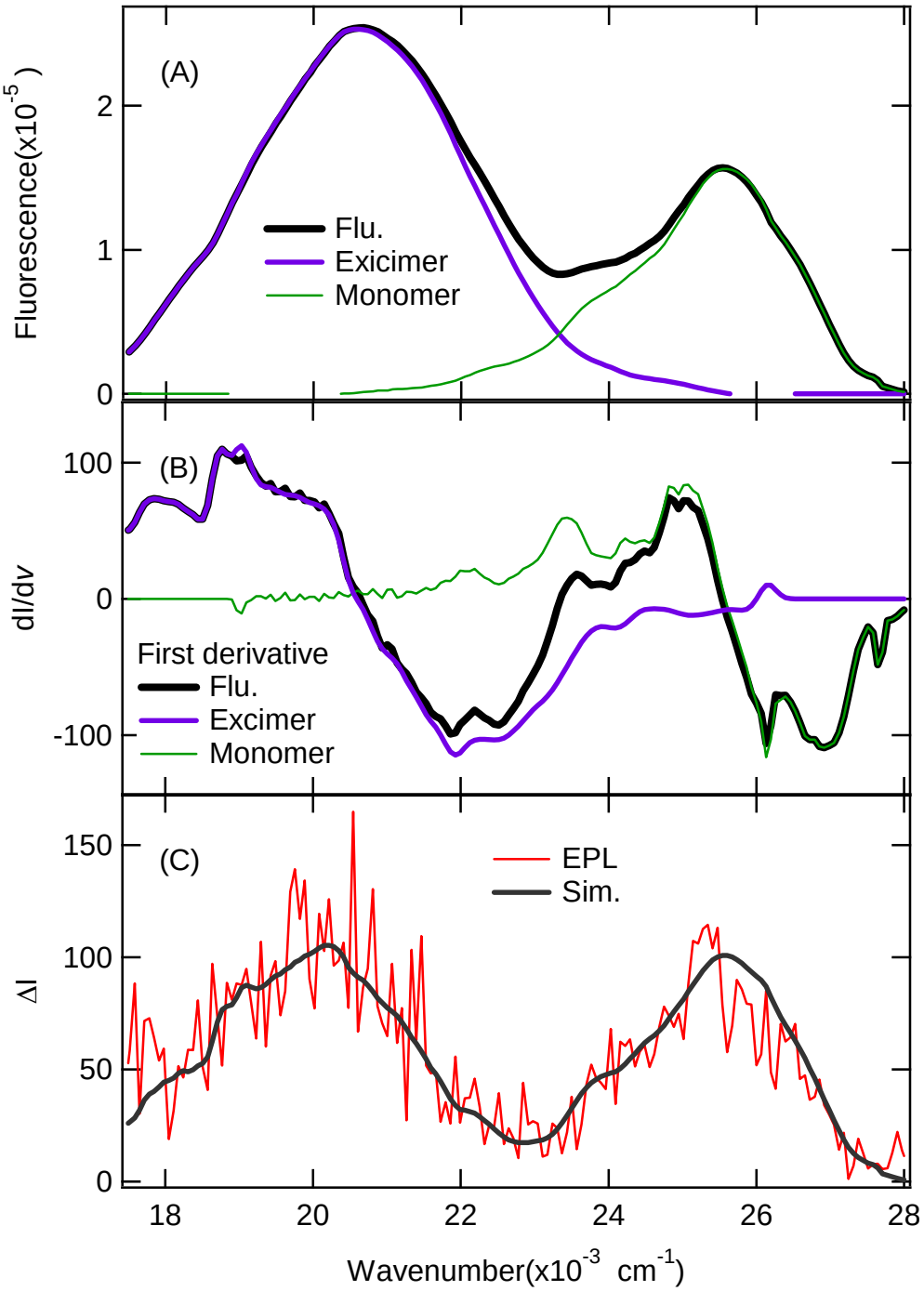

Fig. 4-4. (A) Fluorescence spectrum of pyrene solution 5 x 10^{-3} M. (B) The first derivative spectra of fluorescence bands. (C) E-PL spectrum obtained with field strength 0.2 MVcm^{-1}, and excitation at 30770 cm^{-1}, together with the simulation

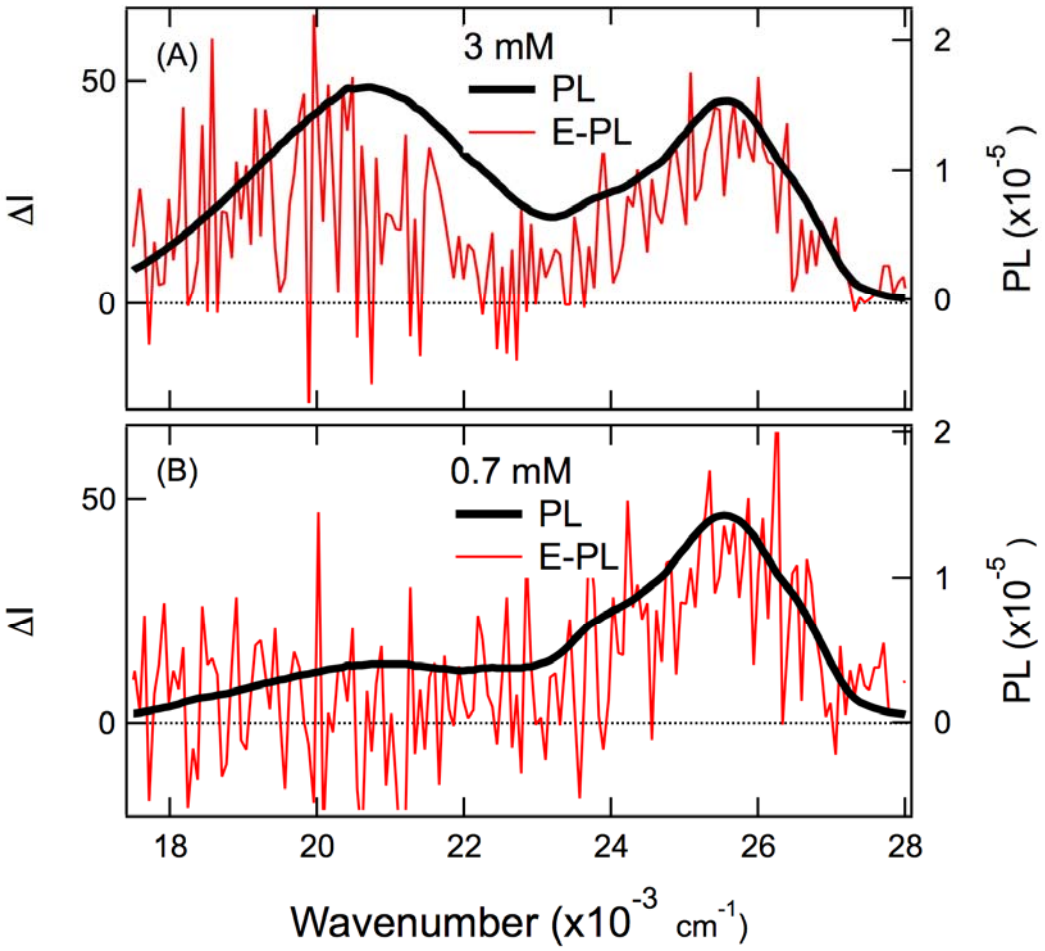

Fig. 4-5. Photoluminescence (PL) spectra (thick line) and E-PL spectra (thin line) of pyrene solution at a concentration of 3 x 10^{-3} M (upper) and 0.7 x 10^{-3} M (lower). Excitation wavelength was 30770 cm^{-1}, and applied field strength was 0.2 $MVcm^{-1}$.

With a steady-state approximation, the quantum yield of monomer fluorescence and excimer fluorescence can be presented as follows [8]:

$$\Phi_M = \frac{k_{f_M} Y}{k_M Y + [c] k_{DM} k_D} \tag{2}$$

$$\Phi_D = \frac{k_{f_D} [c] k_{DM}}{k_M Y + [c] k_{DM} k_D} \tag{3}$$

where $[c]$ is concentration of pyrene, $Y = k_D + k_{MD}$, $k_M = k_{iM} + k_{fM}$ and $k_D = k_{iD} + k_{fD}$. In this model, the time dependence of monomer fluorescence intensity ($I_M(t)$) and excimer fluorescence intensity ($I_D(t)$) can be expressed by a bi-exponential function as follows:

$$I_M(t) = c_1 \exp(-\lambda_1 t) + c_2 \exp(-\lambda_2 t) \tag{4}$$

$$I_D(t) = -c_3 \exp(-\lambda_1 t) + c_3 \exp(-\lambda_2 t) \tag{5}$$

with the following relations: $\lambda_1 + \lambda_2 = k_M + [c] k_{DM} + k_D + k_{MD}$, $\lambda_1 \lambda_2 = [c] k_{DM} k_D + k_M k_{MD} + k_M k_D$. In fact, the decay of monomer fluorescence observed at 5 x 10^{-3} M shows a biexpoential decay and excimer fluorescence shows an arise and decay profile, as shown in Fig. 4-6. At a very low concentration of 5 x 10^{-6} M, where excimer fluorescence is negligible, monomer fluorescence shows a single exponential decay (see Fig. 4-7). Based on the results of the decay measurements, the following rate constants can be determined under the present experimental conditions: k_M =(3.6±0.7) × 10^7 s^{-1}, k_{DM} =(3.9±0.7) × 10^9 s^{-1} $lmol^{-1}$, k_{MD} =(9.2±1.7) × 10^6 s^{-1}, k_D =(5.0±0.9) × 10^7 s^{-1}.

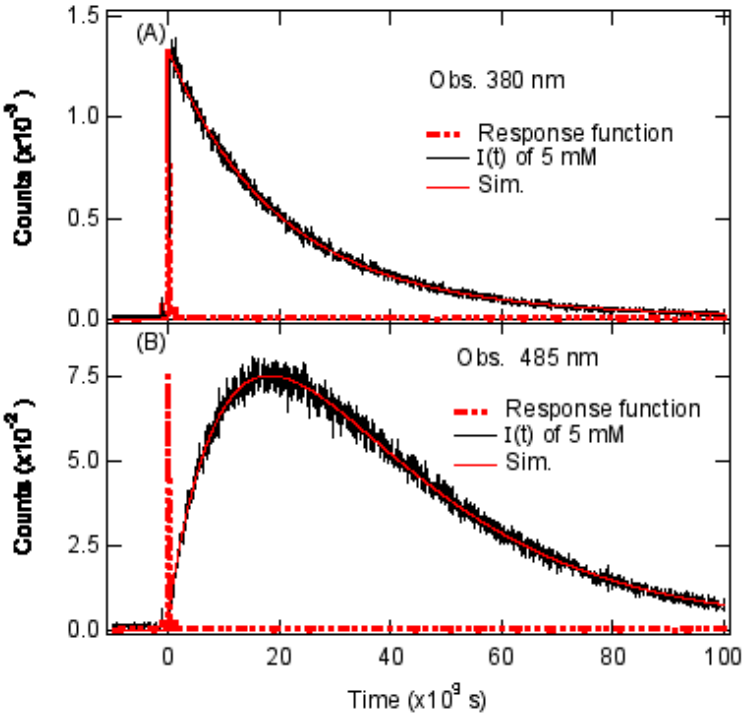

Fig. 4-6 Fluorescence decay of monomer fluorescence at 380 nm (upper) and excimer fluorescence at 485 nm (lower) of pyrene solution at concentration of 5 x 10^{-3} M. Black line shows the observed decay, thin line shows the simulated decay, and chain line shows the response function of the scattered light. Excitation wavelength was 300 nm.

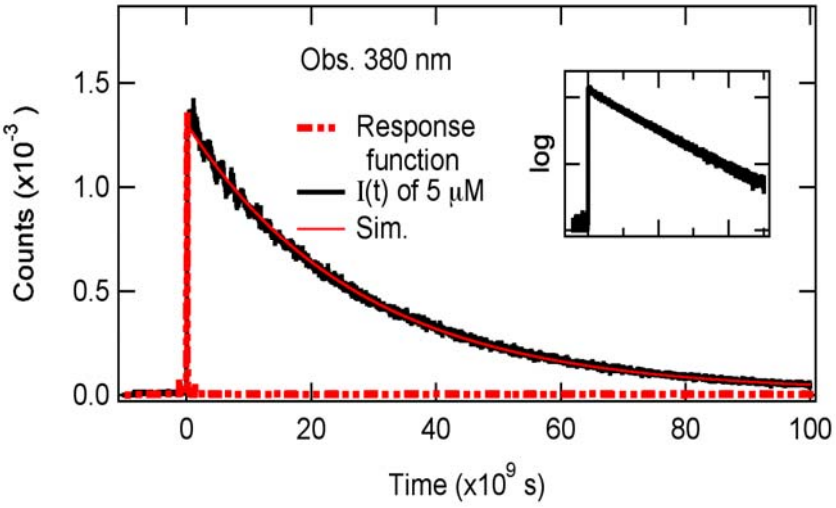

Fig. 4-7. Fluorescence decay of monomer fluorescence of pyrene solution at a low concentration of 5 x 10^{-6} M. The decay in the logarithmic scale is shown in the inlet.

Based on Eqs. (2) and (3), the field-induced change in intensity relative to the total intensity in monomer fluorescence and excimer fluorescence, respectively, i. e., $\Delta I_M/I_M$, and $\Delta I_D/I_D$ can be formulated. With the kinetic model (Birk's model) shown in the text, it is given below how equations can be derived.

(1) $\Delta I_M/I_M$

The quantum yield of monomer fluorescence is expressed in the form

$$\Phi_M = \frac{k_{fM} Y}{k_M Y + [c] k_{DM} k_D} \tag{6}$$

It is assumed that the radiative rate constant (k_{fM}) is independent of the electric field, and the field-induced change in the field-dependence rate constant is denoted by Δk. Then, the fluorescence quantum yield of the monomer fluorescence in the presence of electric field (Φ_M^F) is given by

$$\Phi_M^F = \frac{k_{fM} Y^F}{k_M^F Y^F + [c] k_{DM}^F k_D^F} = \frac{k_{fM}(Y + \Delta Y)}{(k_M + \Delta k_M)(Y + \Delta Y) + [c](k_{DM} + \Delta k_{DM})(k_D + \Delta k_D)} \tag{7}$$

Eq. (7) can be rewritten in the form

$$\Phi_M^F = \frac{k_{fM}(Y + \Delta Y)}{Z + \Delta Z} = \frac{k_{fM}(Y + \Delta Y)}{Z}\left(\frac{1}{1 + \frac{\Delta Z}{Z}}\right) \tag{8}$$

where $Z = k_M Y + [c] k_{DM} k_D$, $\Delta Z = k_M \Delta Y + \Delta k_M (Y + \Delta Y) + [c] k_{DM} \Delta k_D + [c] \Delta k_{DM} (k_D + \Delta k_D)$. It would be reasonable to suppose that $\Delta Z << Z$. By using the relation, $\frac{1}{1-x} = \sum_{n=0}^{\infty} x^n$, and $|x| < 1$, Eq. (8) becomes

$$\Phi_M^F = \frac{k_{fM}(Y+\Delta Y)}{Z}\left(\frac{1}{1-(-\frac{\Delta Z}{Z})}\right) = \frac{k_{fM}(Y+\Delta Y)}{Z}\left(1+(-\frac{\Delta Z}{Z})+(-\frac{\Delta Z}{Z})^2+\cdots\right) \tag{9}$$

We may neglect $(\Delta Z/Z)^n$ with $n \geqq 2$, that is much smaller than $\Delta Z/Z$, and the following relation can be obtained:

$$\Phi_M^F \approx \frac{k_{fM}(Y+\Delta Y)}{Z}(1-\frac{\Delta Z}{Z}). \tag{10}$$

Using Eqs. (6) and (10) we obtain the following expression of $\Delta\Phi_M/\Phi_M$:

$$\frac{\Delta\Phi_M}{\Phi_M} = \frac{\Phi_M^F - \Phi_M}{\Phi_M} = \frac{\frac{k_{fM}(Y+\Delta Y)}{Z}(1-\frac{\Delta Z}{Z}) - \frac{k_{fM}Y}{Z}}{\frac{k_{fM}Y}{Z}} = \frac{\Delta Y}{Y} - \frac{\Delta Z}{Z} - \frac{\Delta Z}{Z}\frac{\Delta Y}{Y}. \tag{11}$$

By assuming that $\Delta Z\Delta Y/YZ$ is relatively small, the $\Delta\Phi_M/\Phi_M$ can be expressed in the form of

$$\frac{\Delta\Phi_M}{\Phi_M} \approx -\frac{\Delta Z}{Z} + \frac{\Delta Y}{Y}. \tag{12}$$

Then, the observed $\Delta I_M/I_M$, which is equivalent to $\Delta\Phi_M/\Phi_M$, can be roughly expressed as follows:

$$\frac{\Delta I_M}{I_M} \approx -(\frac{Y\Delta k_M + k_M\Delta k_{MD} + k_M\Delta k_D + [c]k_{DM}\Delta k_D + k_D[c]\Delta k_{DM}}{Z}) + \frac{\Delta k_{MD} + \Delta k_D}{Y} \tag{13}$$

Further simplification is made for Eq. (13) by assuming that $[c]\Delta k_{DM}\Delta k_D/Z$ and $\Delta k_M\Delta Y/Z$ are negligibly small. Then,

$$\frac{\Delta I_M}{I_M} \approx -\frac{k_D}{Z}[c]\Delta k_{DM} + \frac{[c]k_{DM}k_D}{YZ}\Delta k_{MD} - \frac{[c]k_{DM}k_{MD}}{YZ}\Delta k_D - \frac{Y}{Z}\Delta k_M \tag{14}$$

(2) $\Delta I_D/I_D$

The quantum yield of excimer fluorescence can be represented by

$$\Phi_D = \frac{k_{fD}[c]k_{DM}}{k_M Y + [c]k_{DM}k_D} \tag{15}$$

Then, the yield of excimer fluorescence in the presence of electric field can be given by

$$\Phi_D^F \approx \frac{k_{fD}[c]k_{DM}^F}{k_M^F Y^F + [c]k_{DM}^F k_D^F} = \frac{k_{fD}[c](k_{DM} + \Delta k_{DM})}{(k_M + \Delta k_M)(Y + \Delta Y) + [c](k_{DM} + \Delta k_{DM})(k_D + \Delta k_D)} \tag{16}$$

By rearranging the above equation, the following can be obtained:

$$\Phi_D^F = \frac{k_{fD}[c](k_{DM} + \Delta k_{DM})}{Z + \Delta Z} = \frac{k_{fD}[c](k_{DM} + \Delta k_{DM})}{Z}\left(1 + (-\frac{\Delta Z}{Z}) + (-\frac{\Delta Z}{Z})^2 + \text{L}\right) \tag{17}$$

Then $\Delta\Phi_D/\Phi_D$ can be expressed as

$$\frac{\Delta\Phi_D}{\Phi_D} = \frac{\frac{k_{fD}[c](k_{DM} + \Delta k_{DM})}{Z}(1 - \frac{\Delta Z}{Z}) - \frac{k_{fD}[c]k_{DM}}{Z}}{\frac{k_{fD}[c]k_{DM}}{Z}} = \frac{[c]\Delta k_{DM}}{[c]k_{DM}} - \frac{\Delta Z}{Z} - \frac{\Delta Z}{Z}\frac{[c]\Delta k_{DM}}{[c]k_{DM}} \tag{18}$$

On the assumption that $\Delta Z\Delta k_{DM}/Zk_{DM}$ is relatively small,

$$\frac{\Delta\Phi_D}{\Phi_D} \approx -\frac{\Delta Z}{Z} + \frac{[c]\Delta k_{DM}}{[c]k_{DM}} \tag{19}$$

The observed $\Delta I_D/I_D$, which is equivalent to $\Delta\Phi_D/\Phi_D$, can be expressed with the assumption that $[c]\Delta k_D\Delta k_{DM}/Z$ and $\Delta k_M\Delta Y/Z$ are relatively small:

$$\frac{\Delta I_D}{I_D} \approx -(\frac{Y\Delta k_M + k_M\Delta k_{MD} + k_M\Delta k_D + [c]k_{DM}\Delta k_D + k_D[c]\Delta k_{DM}}{Z}) + \frac{[c]\Delta k_{DM}}{[c]k_{DM}} \tag{20}$$

By rearranging the above equation,

$$\frac{\Delta I_D}{I_D} \approx \frac{k_M Y}{[c]k_{DM}Z}[c]\Delta k_{DM} - \frac{k_M}{Z}\Delta k_{MD} - (\frac{[c]k_{DM} + k_M}{Z})\Delta k_D - \frac{Y}{Z}\Delta k_M \tag{21}$$

A combination between $\Delta I_M/I_M$ and $\Delta I_D/I_D$ gives the following relation:

$$\begin{cases} \dfrac{\Delta I_M}{I_M}\dfrac{k_M Y}{\underline{[c]k_{DM}Z}} = -\dfrac{k_D}{Z}\dfrac{k_M Y}{\underline{[c]k_{DM}Z}}[c]\Delta k_{DM} + \dfrac{[c]k_{DM}k_D}{YZ}\dfrac{k_M Y}{\underline{[c]k_{DM}Z}}\Delta k_{MD} \\ -\dfrac{[c]k_{DM}k_{MD}}{YZ}\dfrac{k_M Y}{\underline{[c]k_{DM}Z}}\Delta k_D - \dfrac{Y}{Z}\dfrac{k_M Y}{\underline{[c]k_{DM}Z}}\Delta k_M \\ \\ \dfrac{\Delta I_D}{I_D}\dfrac{k_D}{\underline{Z}} = \dfrac{k_M Y}{[c]k_{DM}Z}\dfrac{k_D}{\underline{Z}}[c]\Delta k_{DM} - \dfrac{k_M}{Z}\dfrac{k_D}{\underline{Z}}\Delta k_{MD} - (\dfrac{[c]k_{DM}+k_M}{Z})\dfrac{k_D}{\underline{Z}}\Delta k_D - \dfrac{Y}{Z}\dfrac{k_D}{\underline{Z}}\Delta k_M \end{cases} \quad (22)$$

that is,

$$\begin{aligned} &\frac{\Delta I_M}{I_M}\frac{k_M Y}{[c]k_{DM}Z} + \frac{\Delta I_D}{I_D}\frac{k_D}{Z} = -(\frac{k_M k_{MD}}{ZZ} + \frac{k_M k_D + [c]k_{DM}k_D}{ZZ})\Delta k_D \\ &-\frac{Y}{Z}(\frac{k_M Y + [c]k_{DM}k_D}{[c]k_{DM}Z})\Delta k_M \\ &= -(\frac{k_M Y + [c]k_{DM}k_D}{ZZ})\Delta k_D - \frac{Y}{Z}(\frac{Z}{[c]k_{DM}Z})\Delta k_M = -\frac{1}{Z}\Delta k_D - \frac{Y}{Z[c]k_{DM}}\Delta k_M \end{aligned} \quad (23)$$

Then,

$$\Delta k_D + \frac{Y}{[c]k_{DM}}\Delta k_M = -\frac{k_M Y}{[c]k_{DM}}\frac{\Delta I_M}{I_M} - k_D\frac{\Delta I_D}{I_D} \quad (24)$$

As shown in Fig. 4-1, the absorption intensity of pyrene is not affected by application of electric fields, implying that the radiative decay rate of monomer fluorescence is not affected by ***F***. In the analysis, therefore, it may be reasonable to consider that the radiative rate constant both of monomer and of excimer is independent of the applied electric field. The fluorescence quantum yield at low concentrations where excimer fluorescence is negligible is not affected by application of electric field in a solid film of PMMA, suggesting that the total decay rate including radiative and nonradiative decay rates other than the excimer formation rate is independent of the applied electric field in solid films under vacuum conditions.

Then, it may be assumed that k_M, which was obtained to be 3.6 x 10^7 s^{-1} by measuring the decay profile of monomer fluorescence at a low concentration of 5 x 10^{-6} M, is not affected by application of electric fields, i.e., $\Delta k_M = 0$ in Eqs. (14) and (21).

In Eqs. (14) and (21), the signs of the coefficients of Δk_{DM} or Δk_{MD} are opposite to each other, while the coefficient of Δk_D has the same signature. If the field effect of fluorescence intensity results from Δk_{DM} or Δk_{MD}, monomer fluorescence intensity and excimer fluorescence intensity seem to show opposite field effect. As mentioned already, however, both fluorescence emissions are enhanced by application of electric field, implying that the field effect on fluorescence intensity results from the field-induced change in k_D, i.e., Δk_D. If Δk_M can be neglected in Eq. (24), Δk_D is given as follows:

$$\Delta k_D \approx -\frac{k_M Y}{[c]k_{DM}}\frac{\Delta I_M}{I_M} - k_D\frac{\Delta I_D}{I_D} \tag{25}$$

The values of $\Delta I_M/I_M$ and $\Delta I_D/I_D$ as well as their ratio at different concentrations of 3 x 10^{-3} and 5 x 10^{-3} M obtained from the E-PL spectra shown in Fig. 4-2 and 4-5 are given in Table 1. By using those values, Δk_D with a field strength of 0.2 $MVcm^{-1}$ is obtained to be -7.7 x 10^4 s^{-1} and -5.3 x 10^4 s^{-1}, respectively, at a concentration of 5 x 10^{-3} M and 3 x 10^{-3} M (see Table 1). Then, the average value of Δk_D with a field strength of 0.2 $MVcm^{-1}$ is –(6.5 ± 1.2) x 10^4 s^{-1}, suggesting that the field-induced enhancement of monomer and excimer fluorescence comes from the field-induced

deceleration of the nonradiative decay rate at the emitting state of the excimer fluorescence. Note that these values are derived by assuming that $\Delta k_M = 0$. At 0.7 x 10^{-3} M, the field-induced change in monomer fluorescence intensity was confirmed, but the change in excimer fluorescence couldn't be confirmed, though excimer fluorescence can be observed in the PL spectrum, as shown in Fig. 4-5b. If the ratio between $\Delta I_M / I_M$ and $\Delta I_D / I_D$ at 0.7 x 10^{-3} M is nearly the same as the ones at 3 x 10^{-3} M or 5 x 10^{-3} M, i.e., 1.6 or 1.7, $\Delta I_D / I_D$ at 0.7 x 10^{-3} M may be around 1.7 x 10^{-4}. If the peak intensity of the excimer fluorescence at 0.7 x 10^{-3} M is 4 x 10^4, as shown in Fig. 5-5b, the field-induced change in excimer fluorescence intensity is expected to be ~7, which is too small to be detected in the present experiments, since the deviation of the field-induced change is ±10 in the same intensity scale, as seen in Fig. 5-5b. Thus, the present results that the field-induced change in excimer fluorescence is not confirmed at 0.7 x 10^{-3} M are consistent with the present conclusion.

As mentioned above, the field-induced enhancement can be interpreted in terms of the field-induced de-enhancement of the nonradiative decay rate at the emitting state of excimer fluorescence. The present experiments were done at ambient pressure, and the decay rate of the excimer fluorescence was determined to be 5 x 10^7 s^{-1}. Under the vacuum conditions, the decay rate of the excimer fluorescence was reported to be

around 1.55 x 10^7 s^{-1} in cyclohexane at 300 K [7], which is much smaller than the present value of k_D, indicating that the nonradiative process of the fluorescent excimer is mainly attributed to the quenching of the excimer by oxygen dissolved in solution. The decay rate of excimer fluorescence was shown to be enhanced by application of electric field in PMMA under vacuum conditions, where the quenching of the excimer fluorescence by oxygen was not necessary to be considered. Therefore, the present results may suggest that the quenching of the fluorescent excimer state of pyrene by oxygen is de-enhanced by application of electric field. The experiments in solid films showed that the excimer formation process was enhanced by application of electric field. At the moment, however, it is not certain whether excimer formation as well as its reverse process is affected by application of electric fields in solution. With respect to the field effect on the nonradiative decay rate at the emitting state of the monomer fluorescence of pyrene solution in air is also the future problem.

In the above discussion, it is assumed that $\Delta k_M = 0$. It should be mentioned that the nonradiative processes of pyrene of the present sample are different from the ones in PMMA even at the emitting state of monomer fluorescence because the sample was not unable to be degassed in the present experiments, and so the validity of the assumption that $\Delta k_M = 0$ are not certain in the present experiments. When pyrene concentration is very low, the following relation can be obtained:

$$\frac{\Delta I_M}{I_M} = -\frac{\Delta k_M}{k_M} \tag{26}$$

E-PL spectra could not be measured for the samples where the pyrene concentration is low enough to exclude the excimer formation process. If the concentration of 0.7 x 10^{-3} M can be regarded as low enough to exclude the excimer formation process, Δk_M may be estimated to be -8 x 10^3 s^{-1}. If this field effect on k_M is applicable at any concentration, Δk_D is estimated to be -1.3 x 10^4 s^{-1} and -5.4 x 10^4 s^{-1} at 3 and 5 x 10^{-3} M, respectively, as shown in Table 1. The observation of the excimer fluorescence shows the invalidity of the above assumption that the concentration of 0.7 x 10^{-3} M is low enough. However, the above discussion seems to reconfirm that the field-induced de-enhancement of the nonradiative decay rate at the emitting state of excimer fluorescence, which leads to the field-induced enhancement both of monomer fluorescence and excimer fluorescence, is surely correct, irrespective of the field-induced change in nonradiative decay at the emitting state of monomer fluorescence.

Table 1. The magnitude of the field-induced change in fluorescence intensity of each component at different concentrations obtained with a field strength of 0.2 $MVcm^{-1}$, the ratio of the field-induced change between monomer fluorescence and excimer fluorescence, i.e., $(\Delta I_M / I_M)/(\Delta I_D / I_D)$, and the evaluated value of the field-induced change in k_D.

[a][c]	$\Delta I_M/I_M \times 10^4$	$\Delta I_D/I_D \times 10^4$	ratio	[b]$\Delta k_D \times 10^{-4}$ s^{-1}	[c]$\Delta k_D \times 10^{-4}$ s^{-1}
5	5.5±1.5	3.5±1.0	1.6	-7.7±2.2	-5.4±2.1
3	2.5±0.8	1.5±0.5	1.7	-5.3±1.7	-1.3±1.7
0.7	2.2±1.0	–	–	–	–

[a]Concentration in unit of 10^{-3} M.

[b]Assuming that Δk_M=0

[c]Assuming that $\Delta k_M \neq 0$ and that $\frac{\Delta I_M}{I_M} \approx -\frac{\Delta k_M}{k_M}$ at 0.7 x10^{-3} M; Δk_M = -8 ×10^3 s^{-1}

[1] Ohta, N.; Umeuchi, S.; Kanada, T.; Nishimura, Y.; Yamazaki, I, An enhancement of excimer formation rate of pyrene by an external electric field in a PMMA polymer film. *Chem*. *Phys*. *Lett*. **1997**, *279*, 215–222.

[2] Nakabayashi, T.; Morikawa, T.; Ohta, N. Direct measurements of the electric-field-induced change in fluorescence decay profile of pyrene doped in a polymer film. *Chem*. *Phys*. *Lett*. **2004**, *395*, 346–350.

[3] Callis, P. R.; Burgess, B. K. Tryptophan Fluorescence Shifts in Proteins from Hybrid Simulations: An Electrostatic Approach. *J*. *Phys*. *Chem*. *B* **1997**, *101*, 9429–9432.

[4] Park, E. S.; Andrews, S. S.; Hu, R. B.; Boxer, S. G. Vibrational Stark Spectroscopy in Proteins: A Probe and Calibration for Electrostatic Fields. *J*. *Phys*. *Chem*. *B* **1999**, *103*, 9813–9817.

[5] Kriegl, J. M.; Nienhaus, K.; Deng, P.; Fuchs, J.; Nienhaus, G. U. Ligand dynamics in a protein internal cavity. *Proc*. *Natl*. *Acad*. *Sci*. *U.S.A*. **2003**, *100*, 7069–7074.

[6] Umeuchi, S.; Nishimura, Y.; Yamazaki, I.; Murakami, H.; Yamashita, M.; Ohta, N. Electric field effects on absorption and fluorescence spectra of pyrene doped in a PMMA polymer film. *Thin Solid Films* **1997**, *311*, 239–245.

[7] Birks, J. B.; Dyson, D. J.; Munro, I. H. `Excimer' Fluorescence. II. Lifetime Studies of Pyrene Solutions. *Proc*. *R*. *Soc*. *A* **1963**, *275*, 575–588.

Chapter 5
Electric field effect on fluorescence in solutions for methylene linked electron donor and acceptor compounds: carbazole and terephthalic acid methyl ester

5-1 Introduction

The electron transfer in photosynthetic reaction centers, which is ubiquitous and important in nature, has been extensively investigated in physics, chemistry, and biology. Particularly, much work has been done in an effort to understand the mechanism of photo-induced electron transfer in simplified molecular model because such studies provide deep understanding of solar energy conversion. Various synthetic models have been prepared to investigate the electron transfer process. Molecular system where donor and acceptor are attached to chain ends, is highly interesting, because of the fixed distance of two chromophores and of the through-bond charge transfer between two chromophores [1-4]. In the molecular system in which donor and acceptor are bound to methylene chains, rotations about the σ-bonds allow the formation of many different conformations in which the intramolecular excited state complex (exciplex) might take place as has been mentioned.

The mechanism of photo-induced charge transfer can be basically explained as follows:

$D + A \xrightarrow{h\nu} D^* + A$	Photoexcitation	(1)
$D^* + A \rightarrow (D - A)^\dagger$	Delocalization of excited state	(2)
$(D - A)^\dagger \rightarrow (D^{\delta+} - A^{\delta-})^\dagger$	Charge transfer initiation	(3)
$(D^{\delta+} - A^{\delta-})^\dagger \rightarrow (D^+ - A^-)$	Radical-ion pair formation	(4)

$(D^+ - A^-) \rightarrow D^+ - A^-$ Charge separation (5)

where D and A are electron donor and acceptor, respectively. The photo-induced charge transfer is either through bond (intramolecular) or through space (intermolecular), where D and A units are covalently bonded or spatially close to each other without binding, respectively. For intramolecular photo-induced charge transfer, the structure of bonding is an important factor. In addition, due to the large electron dipole moment of radical-ion pair, the charge transfer process can be considerably influenced by the external electric field.

There are number of experimental and theoretical studies concerning the electric field effect on photo-induced charge transfer [5-7]. Spectroscopic studies of the field effect on the electron transfer process have been studied by electrophotoluminescence (E-PL) spectroscopy i.e., by the measurements of the field-induced change in photoluminescence spectrum. This technique has been applied to examine dynamics in the excited state as well as electronic structure in a variety of molecular systems in solution and film. The E-PL measurements of molecular systems composed of carbazole electron donor and electron acceptor such as terephthalic acid methyl ester has been done in polymer solid films [5,6]. As shown in Fig. 5-1, remarkable E-PL signals have been observed, depending both on the electric field strength and on the donor-acceptor distance in PMMA. At all the concentrations, fluorescence emitted

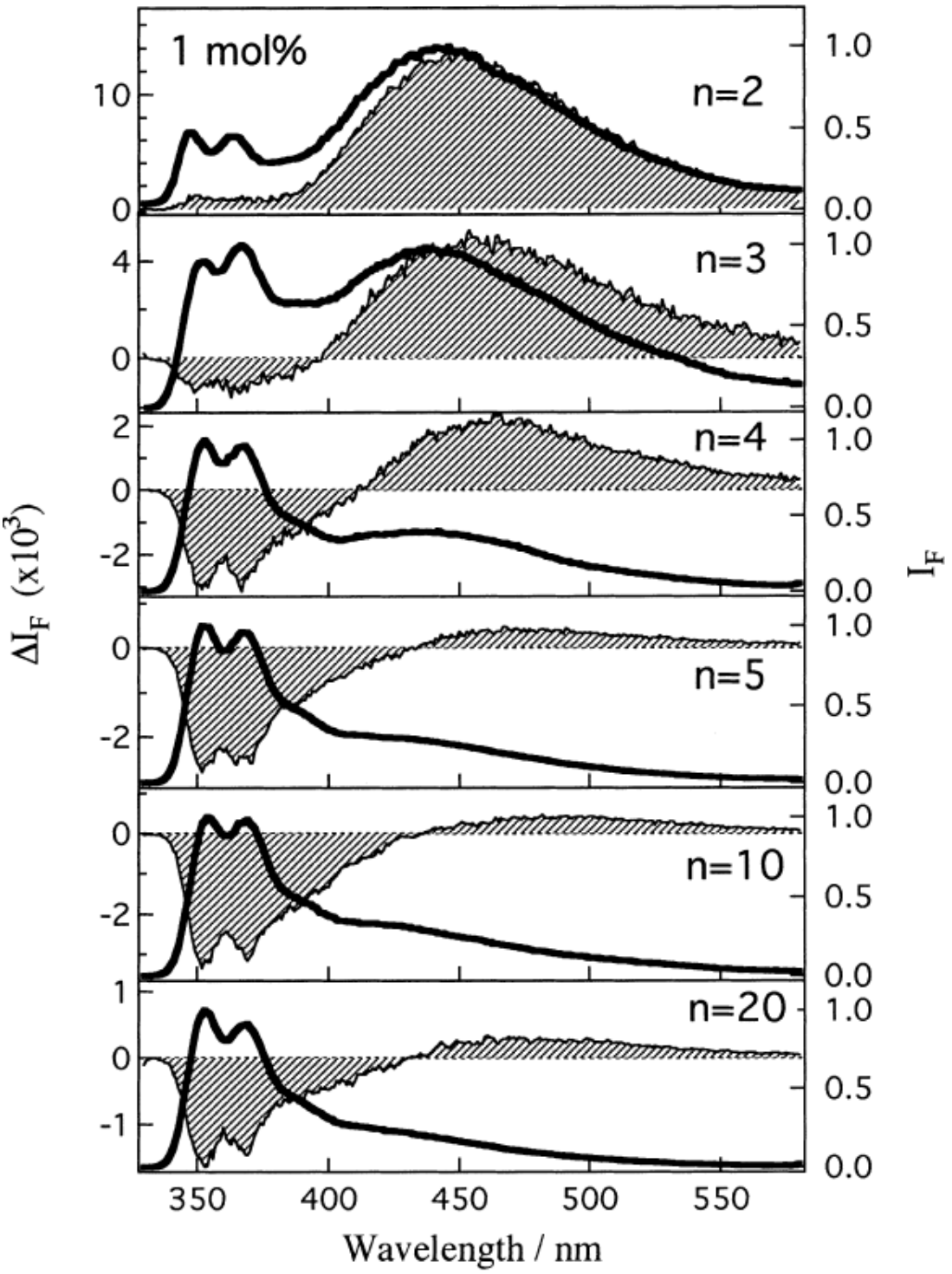

Fig. 5-1 Fluorescence spectra and E-PL spectra of D-(n)-P with n from 2 to 20 doped in a PMMA film at 1.0 mol%. Applied field strength was 0.6 $MVcm^{-1}$ [8].

from the locally excited state of donor carbazole, hereafter noted as monomer fluorescence, is quenched by the electric field and the magnitude increased with increasing the concentration. The exciplex fluorescence is enhanced in PMMA as the concentration is low. These results were interpreted in terms of field effects on electron transfer and on charge recombination processes.

When the samples are doped in polymer solid films, the analysis of the field effect is complicated because of the inhomogeneous distribution. Also the reorientation effect is vanished in the immobile phase. In the present study, polarized E-PL spectra of (carbazole)-$(CH_2)_n$-(terephthalic acid methyl ester) (n = 2-20), where the chemical structure is shown below, were obtained in solution by using an electric-field modulation spectroscopy. The molecular system was composed of carbazole as the electron donor and terephthalic acid methyl ester as the electron acceptor. Hereafter these compounds are denoted as C-(n)-P, where C, n and P indicating carbazole moiety, the number of methylene units and terephthalic acid methyl ester moiety, respectively. The significant angle dependent field-induced change in fluorescence intensity of monomer and exciplex was observed. The experimental results are explained in terms of Liptay model and a kinetic model which is used to explain the emission property of methylene linked D-A compounds in solution.

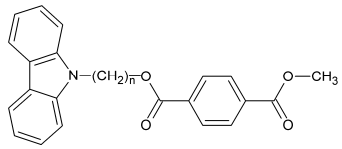

5-2 Material

The concentration of all the samples of C-(n)-P dissolved in decalin (Kanto Chem.) was 5 x 10^{-4} M. The modulation frequency of the applied electric field was 4 kHz and the field strength was 0.2 MV/cm. In the present experiments in solution, the optical measurements are done in the atmospheric condition.

5-3 Results and Discussion

Fig. 5-2 shows absorption spectra of C-(n)-P in solution. All these compounds show similar absorption band in the region from 270 to 360 nm. The bands at 345 and 292 nm are assigned as the transition from the ground state to the S_1 and S_2 states of monomer, respectively. Fluorescence spectra of C-(n)-P show two components: (1) a structured fluorescence in the region from 330-450 nm, which is assigned as monomer fluorescence; (2) a broad emission with a peak at ~415 nm, which is assigned as fluorescence emitted from exciplex as shown in Fig. 5-3. Note that PL spectrum at a concentration of 5 x 10^{-3} M shows the similar structure to the one at 5 x 10^{-4} M, indicating that the intermolecular exciplex can be neglected in these samples. The largest fraction of exciplex emission for C-(3)-P indicates that the linked compound with n=3 forms the most favorable conformation for intramolecular

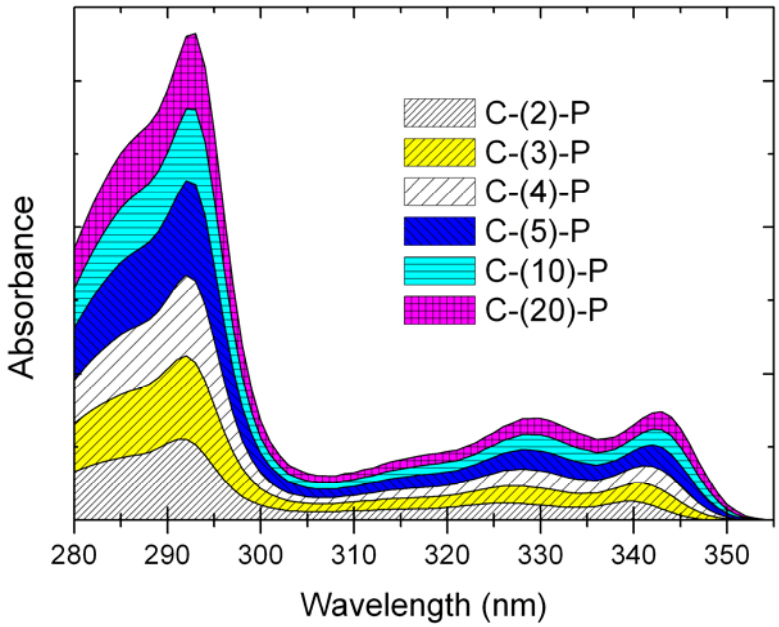

Fig. 5-2 Absorption spectra of C-(n)-P with n from 2 to 20. Concentrations are 0.5 mM for all samples.

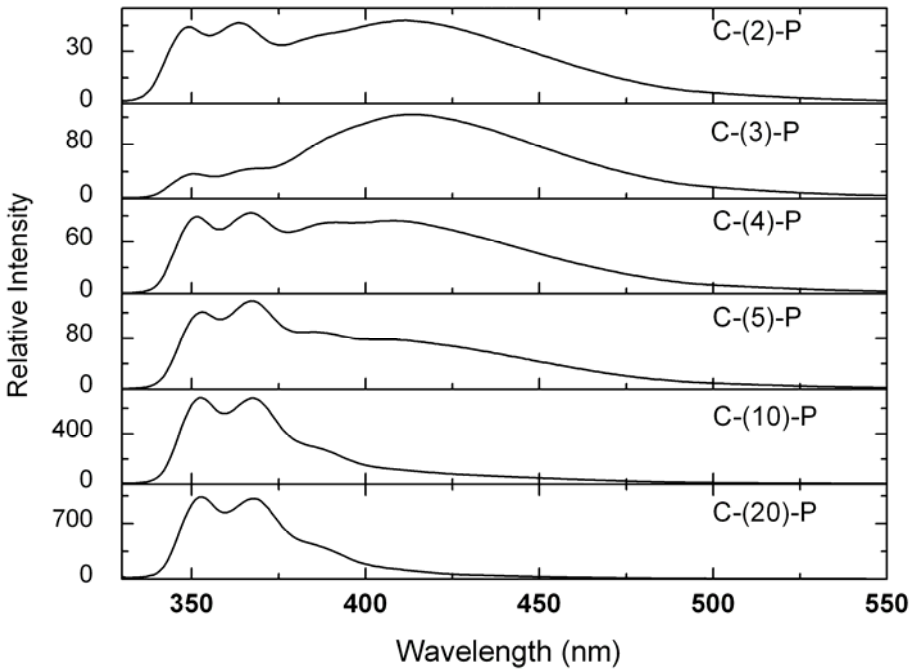

Fig. 5-3 Fluorescence spectra of C-(n)-P dissolved in decalin with excitation wavelength 292 nm. Concentrations are 0.5 mM for all the samples.

exciplex formation. In the compounds having longer methylene chain i.e., in C-(10)-P and C-(20)-P, exciplex fluorescence is relatively weak, probably because C and P moieties are located with long distance. Fig.5-(4-9) shows E-PL spectra of the linked compounds obtained with a field strength of 0.2 $MVcm^{-1}$ at the normal angle (χ=90^o) and magic angle (χ=55^o). The excitation light wavelength was 292 nm, where the field-induced change in absorbance is negligibly small. The field-induced change in fluorescence quantum yield of monomer and exciplex emissions is observed. In addition to the field-induced change in intensity, the exciplex fluorescence is shifted with ***F***. The E-PL spectra could be reproduced by a linear combination of the zeroth and first derivatives of monomer and exciplex fluorescence spectra, as shown in Fig.5-(4-9). At the normal angle of χ, both monomer fluorescence and exciplex fluorescence are quenched. At the magic angle of χ, on the other hand, exciplex fluorescence shows a field-induced enhancement in every compound. Monomer fluorescence is also enhanced by application of electric field in the compounds with n=2, 3. When n is larger than 4, monomer fluorescence of the linked compounds is quenched by application of electric field. Field-induced quenching in monomer fluorescence i.e., $|\Delta I_M/I_M|$ decreases with increasing the chain length from n=4 to 20. The ratio of the field-induced change in quantum yield to fluorescence intensity i.e., $\Delta I/I$ as a function of n is shown in Fig. 5-10. As the origin of the field-induced change

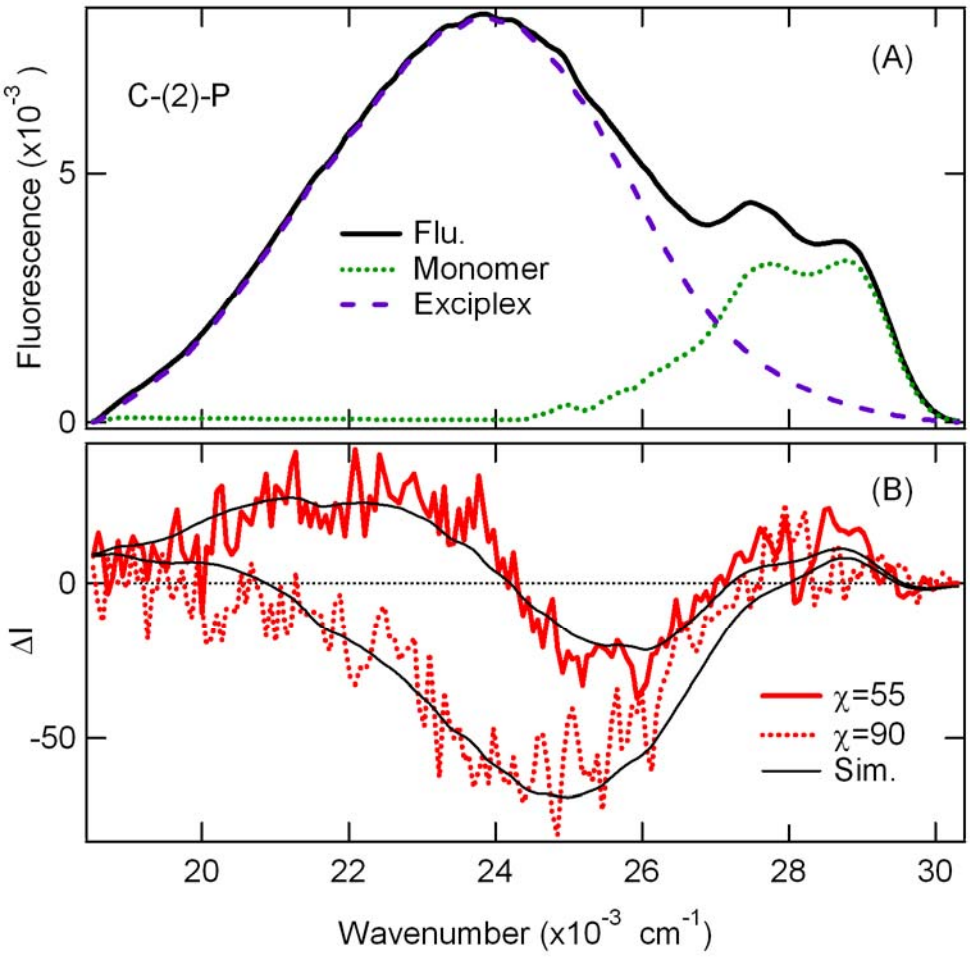

Fig. 5-4 (A) Fluorescence spectra, (B) E-PL spectra observed at χ=55^{o} and 90^{o},and simulation for C-(2)-P

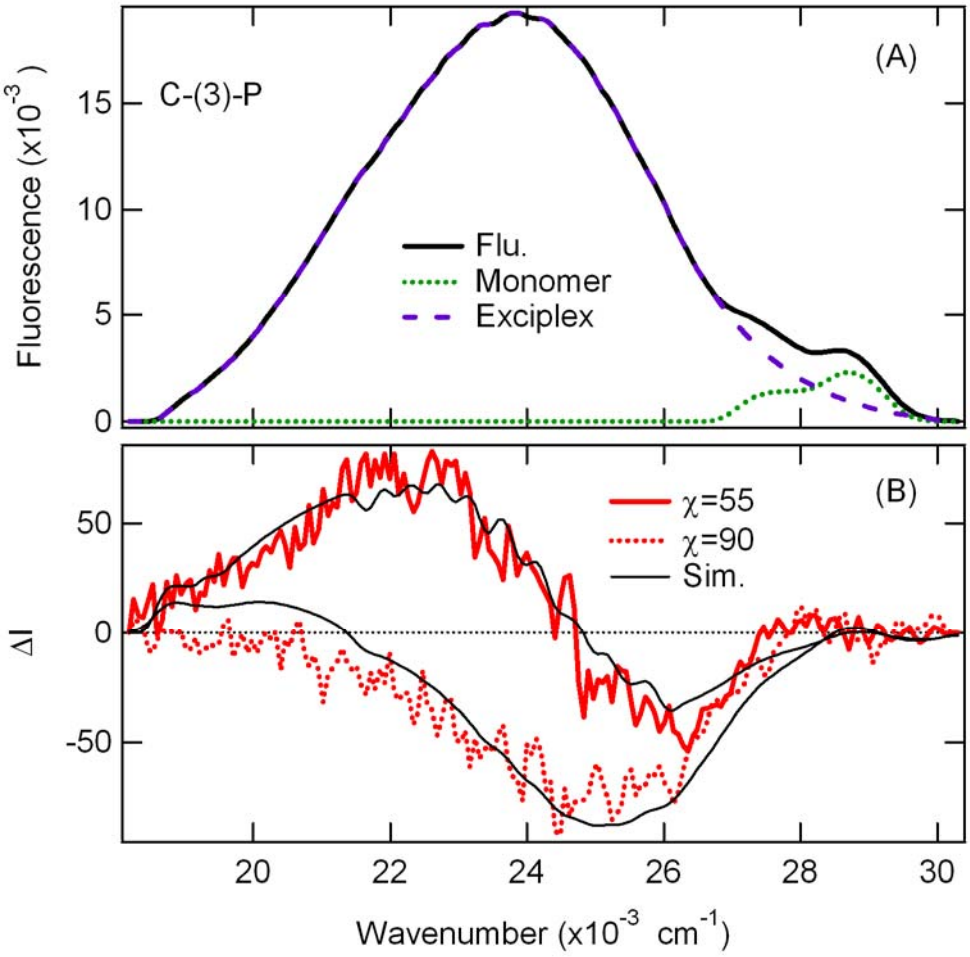

Fig. 5-5 (A) Fluorescence spectra, (B) E-PL spectra observed at χ = 55^{o} and 90^{o}, and simulation for C-(3)-P.

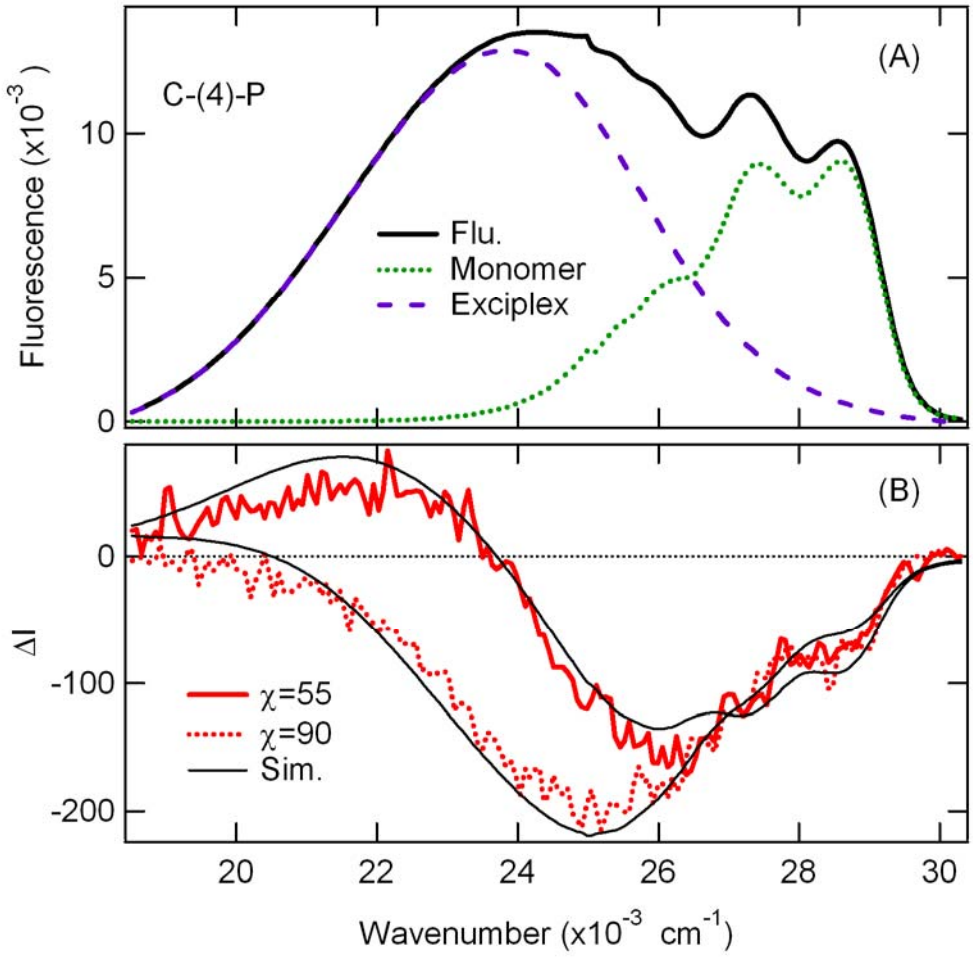

Fig. 5-6 (A) Fluorescence spectra, (B) E-PL spectra observed at χ=55^{o} and 90^{o}, and simulation for C-(4)-P.

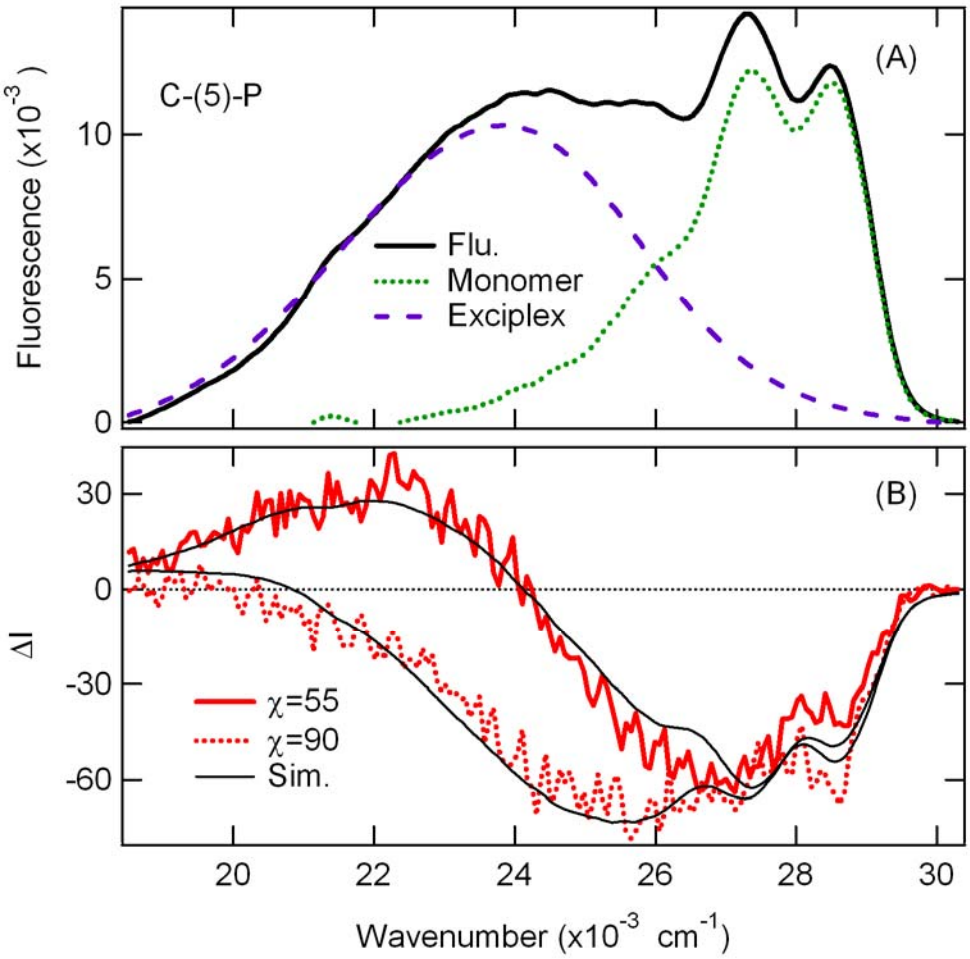

Fig. 5-7 (A) Fluorescence spectra, (B) E-PL spectra observed at χ = 55^{o} and 90^{o}, and simulation for C-(5)-P.

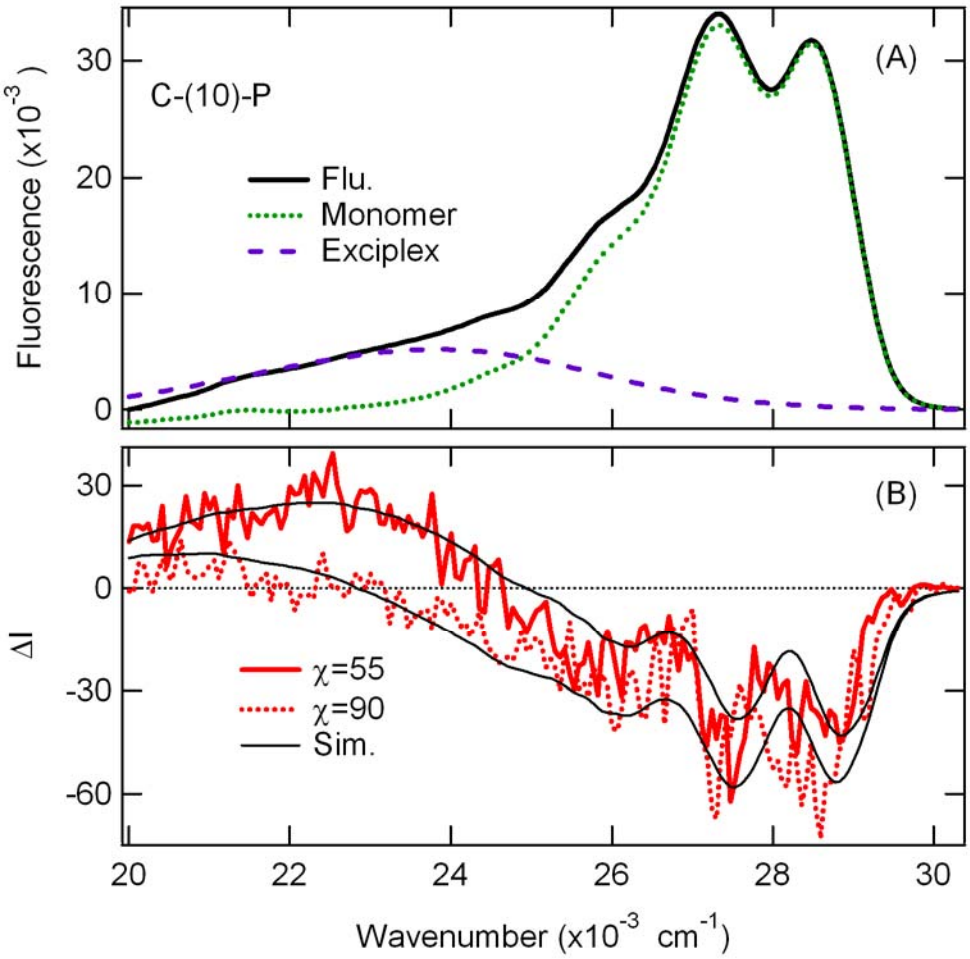

Fig. 5-(A) Fluorescence spectra, (B) E-PL spectra observed at χ = 55^{o} and 90^{o}, and simulation for C-(10)-P.

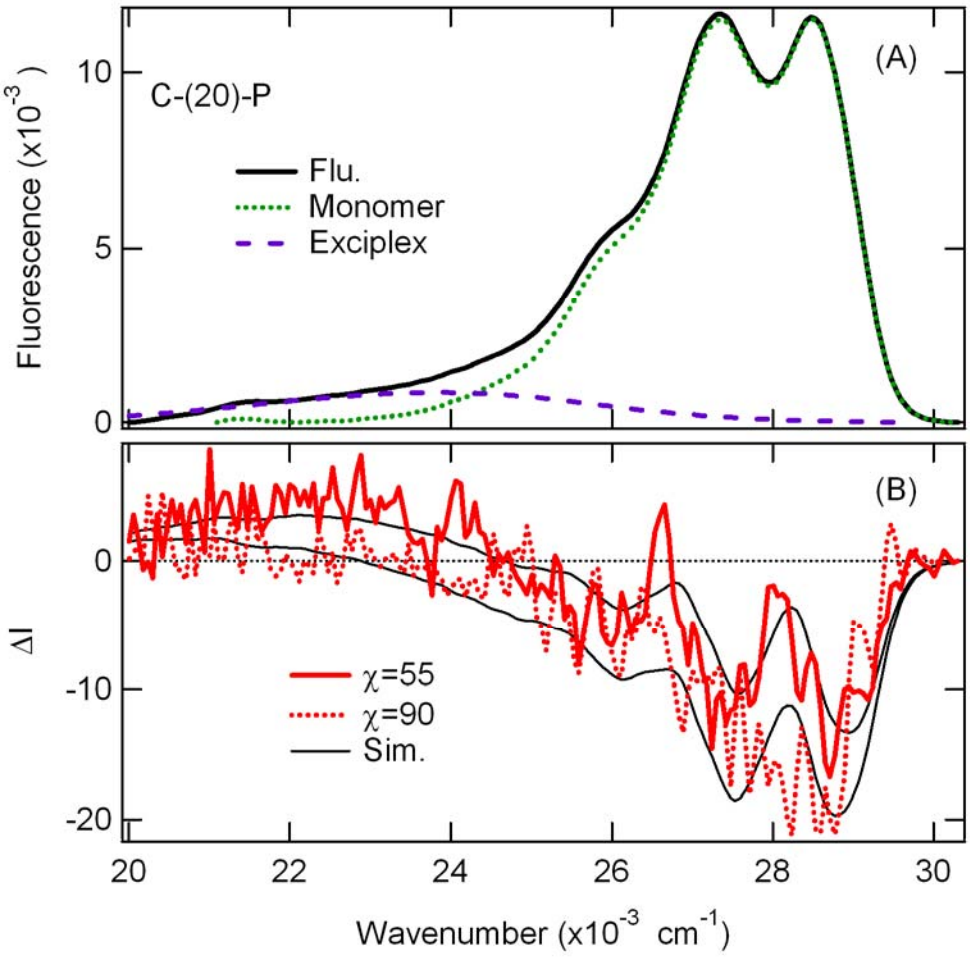

Fig. 5-9 (A) Fluorescence spectra, (B) E-PL spectra observed at χ = 55^{o} and 90^{o}, and simulation for C-(20)-P .

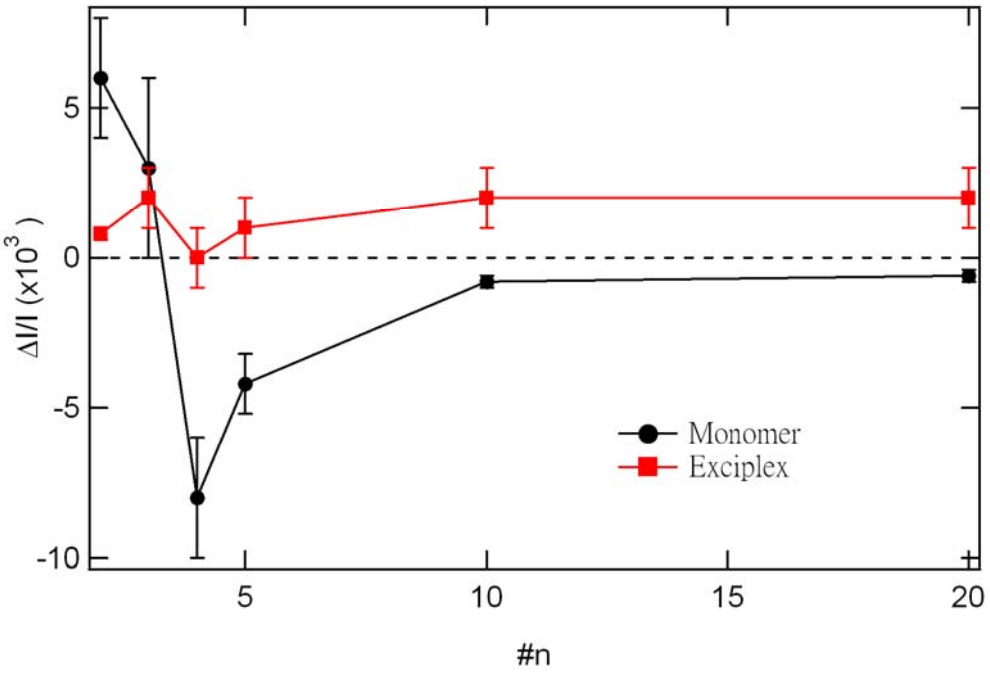

Fig. 5-10 The zeroth order derivative components of E-PL spectra of C-(n)-P at magic angle. The number of methylene chain units is denoted by n.

in fluorescence intensity, two mechanisms can be considered: (1) field-induced change in excitation dynamics; (2) field-induced reorientation of molecules. The former effect is considered to be independent on χ, while the latter effect is considered to be neglected in the E-PL spectra observed at χ=55^{o}. From the difference in the zeroth derivative component between the E-PL spectra observed at the normal and magic angle the dipole moment of the emitting species can be estimated. By assuming that the angle between the electric dipole moment and the transition dipole moment is zero, $\boldsymbol{\mu} \angle \boldsymbol{d}$=0, and that the polarizability terms are negligible, the electric dipole moment of the fluorescent exciplex is estimated to be ~19 D in any n, and the electric dipole moment of the fluorescent monomer is estimated to be ~5.5 D in n=10, 20. It is worth noting that the electric dipole moment in the fluorescent exciplex with n=1-5 is estimated to be 16-17 D based on the solvatochromism [9]. The experimental value of the coefficients used to simulate the observed E-PL spectra is listed in Table 5-1.

The field-induced change in fluorescence intensity observed at χ=55^{o} can be ascribed to the field-induced change in dynamics following photoexcitation. The most simple kinetic model to describe the formation and deactivation of radical-ion pair in methylene linked D-A compounds is represented by,

Table 5-1 Coefficients are used to simulate the E-PL spectra

	C-(2)-P	C-(3)-P	C-(4)-P	C-(5)-P	C-(10)-P	C-(20)-P
Monomer						
$A_{90°}$	$6(\pm1)\times10^{-3}$	$7(\pm3)\times10^{-3}$	$-4(\pm3)\times10^{-3}$	$-4(\pm1)\times10^{-3}$	$-9(\pm4)\times10^{-4}$	$-9(\pm3)\times10^{-4}$
$B_{90°}$	--	--	--	0(±1)	0.6(±0.4)	0.6(±0.2)
$A_{54.7°}$	$6(\pm1)\times10^{-3}$	$3(\pm3)\times10^{-3}$	$-8(\pm2)\times10^{-3}$	$-4(\pm1)\times10^{-3}$	$-8(\pm2)\times10^{-4}$	$-6(\pm2)\times10^{-4}$
$B_{54.7°}$	--	--	--	0(±1)	0.6(±0.4)	0.6(±0.2)
Exciplex						
$A_{90°}$	$-7(\pm1)\times10^{-3}$	$-3(\pm1)\times10^{-3}$	$-1(\pm1)\times10^{-2}$	$-5(\pm1)\times10^{-3}$	$-2(\pm1)\times10^{-3}$	$-2(\pm1)\times10^{-3}$
$B_{90°}$	13(±1)	8(±1)	19(±1)	7(±2)	9(±3)	14(±3)
$A_{54.7°}$	$8(\pm2)\times10^{-4}$	$2(\pm1)\times10^{-3}$	$0(\pm1)\times10^{-3}$	$1(\pm1)\times10^{-3}$	$2(\pm1)\times10^{-3}$	$2(\pm1)\times10^{-3}$
$B_{54.7°}$	13(±1)	8(±2)	19(±4)	7(±2)	9(±4)	14(±5)

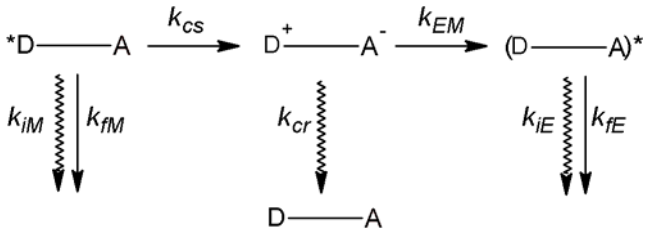

k_{cs} is the rate constant of charge transfer; k_{fM} and k_{fE} are the radiative rate constants of excited monomer and exciplex, respectively; k_{iM} and k_{iE} are the nonradiative rate constants of excited monomer and exciplex, respectively. k_{cr} is the rate constant of the recombination of radical-ion pair into the ground state. k_{EM} is the exciplex formation rate. Fluorescence decays of C-(n)-P were observed at 355 nm (monomer fluorescence) and 450 nm (exciplex fluorescence) with excitation at 292 nm. The results are shown in Figs. 5-11 and 5-12. The exciplex fluorescence decay curves show a rise and decay profile, and monomer fluorescence shows a multiexponential decay. It is clearly seen that the lifetime of the monomer fluorescence decreases with decreasing n, indicating that the electron transfer becomes faster with decreasing chain length. All the decay profiles of monomer fluorescence are fitted by assuming a triexponential decay,

$$I_M(t) = a_1 \exp(-t/\tau_1) + a_2 \exp(-t/\tau_2) + a_3 \exp(-t/\tau_3) \quad (6)$$

where a_i and τ_i are pre-exponential factor and lifetime of component i, respectively. Fitted results of the decay profiles and average lifetime ($\bar{\tau}$), which is given by

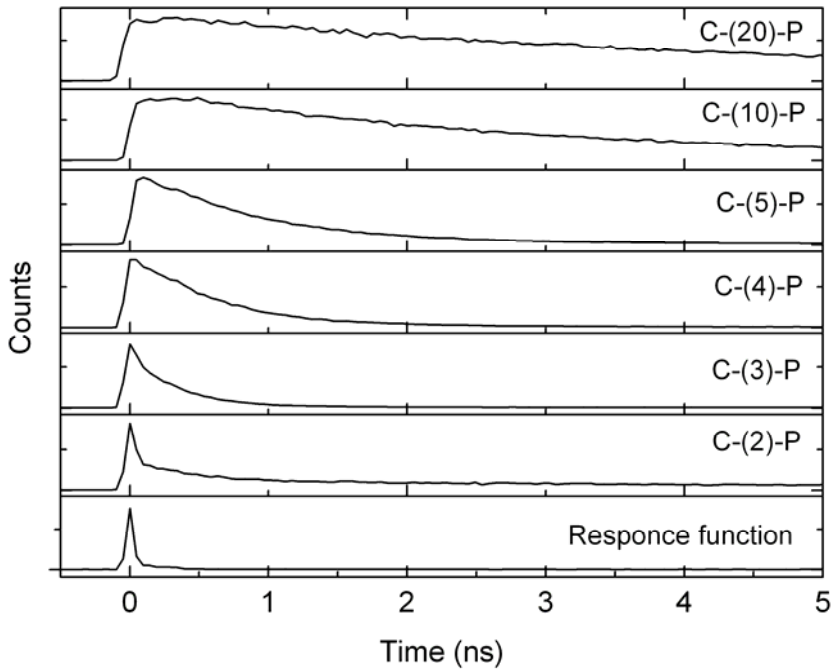

Fig. 5-11 Fluorescence decay curves of C-(n)-P observed at 355 nm. The excitation light wavelength was 292 nm.

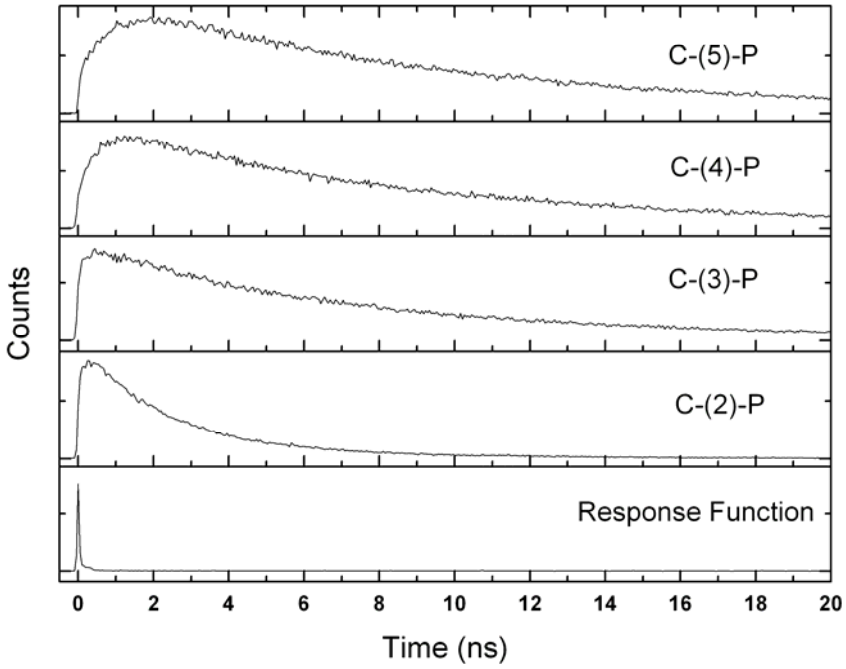

Fig. 5-12 Fluorescence decay curves of C-(n)-P observed at 450 nm. The excitation light wavelength was 292 nm.

$$\int tI(t)dt / \int I(t)dt \tag{7}$$

$$\sum_i a_i \tau_i / \sum_i a_i \tag{8}$$

are shown in Table 5-2. In the decay profiles of the monomer fluorescence with n=2, 3, the overlap of monomer fluorescence with exciplex fluorescence makes it difficult to determine the exact decay and lifetime.

By assuming that the relaxation process of excited monomer is irreversible, the total quantum yield of monomer fluorescence can be expressed as follows:

$$\Phi_M = \frac{k_{fM}}{k_{fM} + k_{iM} + k_{cs}} \tag{10}$$

By assuming that only the electron transfer rate is influenced by the external electric field, the quantum yield of the monomer fluorescence in the presence of electric field is given by

$$\Phi^F = \frac{k_{fM}}{k_{fM} + k_{iM} + (k_{cs} + \Delta k_{cs})} \tag{11}$$

where Δk denotes the field-induced change in rate constants. Suppose that $\bar{\tau}$ (Eq. 8) is given by $\frac{1}{k_{fM} + k_{iM} + k_{cs}}$. The Δk_{cs} can be approximating expressed by the observed field-induced change in fluorescence intensity of monomer $\Delta I_M/I_M$, which is equivalent to $\Delta\Phi/\Phi$:

$$\Delta k_{cs} \approx -\frac{\Delta I_M}{I_M} / [(1 + \frac{\Delta I_M}{I_M})\bar{\tau}] \tag{12}$$

Table 5-2 Fluorescence life time and pre-exponential factor in fluorescence decay of C-(n)-P. Pre-exponential factor of each component is given in parenthesis

[#]n	τ_1 (ns)	τ_2 (ns)	τ_3 (ns)	[a] $\bar{\tau}$ (ns)	[b] $\bar{\tau}$ (ns)
2	0.12 (0.916)	6.3 (0.079)	57 (0.005)	0.88	21
3	0.17 (0.993)	6.3 (0.006)	57 (0.000)	0.25	10
4	0.46 (0.986)	6.3 (0.012)	57 (0.002)	0.63	9.9
5	0.68(0.981)	6.3 (0.018)	57 (0.001)	0.83	5.8
10	2.45 (0.947)	6.3 (0.050)	57 (0.003)	2.81	6.3
20	4.76 (0.960)	6.3 (0.032)	57 (0.008)	5.22	9.3

[a] $\sum_i a_i\tau_i / \sum_i a_i$ is used.

[b] $\int tI(t)dt / \int I(t)dt$ is used.

Then, the Δk_{cs} could be estimated from the E-PL spectra observed at χ=55°. The obtained Δk_{cs} are as follows: -6.8×10^{6} (n=2), -1.2×10^{7} (n=3), 1.3×10^{7} (n=4), 5.1×10^{6} (n=5), 2.9×10^{5} (n=10) and 1.2×10^{5} (n=20) s^{-1} as shown in Table 5-3.

In the Marcus theory of electron transfer, the rate constant k_{cs} is given as follows [10]:

$$k_{cs} = \frac{4\pi^2}{h}\frac{J^2}{(4\pi k_B T\lambda)^{1/2}}\exp[-\frac{(\Delta G+\lambda)^2}{4k_B T\lambda}] \tag{13}$$

where J, h, k_B, T and ΔG represent the transfer integral, Planck's constant, Boltzmann constant, temperature and free energy difference of the reaction, respectively. λ is total reorganization energy. External electric field shifts the energy level of the product, that is, the radical-ion pair, while the field-induced shift is small. The field dependence of free energy results from the interaction between external electric field and the electric dipole moment of the produced radical-ion pair, which is given below.

$$\Delta G^F = \Delta G + \delta G \tag{14}$$

By assuming that only ΔG is affected by electric field, k_{cs} in the presence of electric field is given by

$$k_{cs}^F = k_{cs} + \Delta k_{cs} = \frac{4\pi^2}{h}\frac{J^2}{(4\pi k_B T\lambda)^{1/2}}\exp[-\frac{(\Delta G+\delta G+\lambda)^2}{4k_B T\lambda}] \tag{15}$$

If δG is very small, the second order and higher order terms i.e., $(\delta G)^n$, $n \geqq 2$ can be neglected. Then, Δk_{cs} is given by

$$\Delta k_{cs} = -\frac{2(\Delta G+\lambda)\delta G}{4k_B T\lambda}k_{cs} \tag{16}$$

Table 5-3 Field-induced change, average lifetime and field-induced change in electron transfer rate of C-(n)-P

[#]n	[a]$\Delta I_M/I_M$	[b]$\bar{\tau}$ (ns)	Δk_{cs} (s^{-1})
2	6×10^{-3}	0.88	-6.8×10^{6}
3	3×10^{-3}	0.25	-1.2×10^{7}
4	-8×10^{-3}	0.63	1.3×10^{7}
5	-4×10^{-3}	0.83	5.1×10^{6}
10	-8×10^{-4}	2.81	2.9×10^{5}
20	-6×10^{-4}	5.22	1.2×10^{5}

[a] The zeroth component of E-PL spectra observed at magic angle.

[b] $\sum_i a_i\tau_i / \sum_i a_i$ is used.

By assuming that δG is equal to <-**μ**·**F**>

$$< -\boldsymbol{\mu} \cdot \mathbf{F} >=< -\mu F \cos\theta f(\theta) >=< -\mu F \cos\theta (1 + \frac{\mu F}{k_B T} \cos\theta) >= -\frac{1}{3} \frac{\mu^2 F^2}{k_B T} \quad (17)$$

where $\mu=er$ represents dipole moment of the radical- ion pair, e is the elementary charge and r represents the center-to-center distance between D and A. $f(\theta)$ is the probability of the dipole moment to be found in the direction θ with respect to the applied electric field. Then, the Δk_{cs} can be theoretically estimated:

$$\Delta k_{cs} \approx \frac{1}{6} \frac{\mu^2 F^2 (\Delta G + \lambda)}{k_B^2 T^2 \lambda} k_{cs} \quad (18)$$

By assuming planar zigzag conformation of the methylene chain, the upper limit for the center-to-center distance between D and A is estimated to be ca. 8.3, 9.3, 10.8, 12.0 and 18.3 Å for n= 2, 3, 4, 5, 10, respectively and assuming k_{cs} is ~$1/\tau_1$. The value $(\Delta G + \lambda)/\lambda$ can be estimated to be -0.011, -0.023, 0.049, 0.023 and 0.002 for n= 2, 3, 4, 5, 10, respectively. These values can be used as a test for theoretical model of electron transfer to improve the quantitative prediction.

[1] F. C. De Schryver, N. Boens, and J. Put, in *Adv. Photochem*., ed by J. N. Pitts, Jr., G. S. Hammond, and K. Gollnick, John Wiley & Sons, New York 1977, Vol. 10, p. 359.

[2] a) P. Pasman, F. Rob, and J. W. Verhoeven, Intramolecular charge-transfer absorption and emission resulting from through-bond interaction in bichromophoric molecules. *J. Am. Chem. Soc*., **1982**, *104*, 5127-5133. b) M. N. Paddon-Row, A. M. Oliver, J. M. Warman, K. J. Smit, M. P. de Haas, H. Oevering, and J. W. Verhoeven, Factors affecting charge separation and recombination in photoexcited rigid donor-insulator-acceptor compounds. *J. Phys. Chem.*, **1988**, *92*, 6958-6962.

[3] N. Mataga, Photochemical charge transfer phenomena - picosecond laser photolysis studies. *Pure Appl. Chem.*, **1984**, *56*, 1255-1268.

[4] M. R. Wasielewski, Photoinduced electron transfer in supramolecular systems for artificial photosynthesis. *Chem. Rev*., **1992**, *92*, 435-461.

[5] N. Ohta, M. Koizumi, S. Umeuchi, Y. Nishimura, and I. Yamazaki, External Electric Field Effects on Fluorescence in an Electron Donor and Acceptor System: Ethylcarbazole and Dimethyl Terephthalate in PMMA Polymer Films. *J. Phys. Chem.* **1996**, 100, 16466.

[6] N. Ohta, S. Umeuchi, Y. Nishimura, and I. Yamazaki, Electric-Field-Induced Quenching of Exciplex Fluorescence and Photocurrent Generation in a Mixture of Ethylcarbazole and Dimethyl Terephthalate Doped in a PMMA Polymer Film. *J. Phys. Chem. B* **1998**, 102, 3784.

[7] M. Hilczer, S. Traytak and M. Tachiya, Electric field effects on fluorescence

quenching due to electron transfer. *J. Chem. Phys.* **2001**, 115, 11249.

[8] N. Ohta, Electric Field Effects on Photochemical Dynamics in Solid Films. *Bull. Chem. Soc. Jp*n.*,* **2002**, 75, 1637.

[9] De Schryver, F. C.; Boens, N.; Put, Excited state behavior of some bichromophoric systems.*J. Adv. Photochem*. **1977**, *10*, 359-465.

[10] Marcus, R. A. On the Theory of Oxidation-Reduction Reactions Involving Electron Transfer. *J. Chem. Phys.* **1956**, 24, 966.

Chapter 6
Conclusion

In this thesis, the author measured E-A and E-PL spectra of optoelectronic functional materials in solution by using electric field modulation spectroscopy with the constructed liquid cell and measurement system. The compounds that have been studied are 4-*N*,*N*-dimethylamino-4'-*N*'-methyl-stilbazolium tosylate abbreviated as DAST, pyrene and (carbazole)-$(CH_2)_n$-(terephthalic acid methyl ester) abbreviated as C-(n)-P. The outcomes of the present thesis are summarized as follows:

In chapter 3, the author reports the electric field effects on absorption spectra of DAST microcrystals in dispersion liquid by using E-A spectroscopy. The polarized E-A spectra of DAST microcrystals were obtained and simulated with the absorption spectrum deconvoluted with photoluminescence excitation spectrum into three bands (b1, b2, b3). It is found that b2 band is similar to the absorption band of a single crystal thin film. The b1 and b3 bands may be ascribed to a polydomain structure of microcrystal, which is different from the bulk single crystal. The magnitude of the dipole moment in the ground state was evaluated to be as be as large as $\sim 3\times 10^4$ D for DAST microcrystals having a diameter of 0.35 μm. The measured dipole moment is much less than the value estimated from a theoretical calculation. The difference in the dipole moment between the ground state and excited state and the transition moment of the DAST microcrystal is also found to be affected by application of electric fields. It is found that the ground state dipole moment is irrespective of

molecular arrangements in microcrystals. On contrary, the transition moment depends on the structure of microcrystal.

In chapter 4, the author reports E-PL spectra and E-A spectra of pyrene in solution. The E-A spectra of pyrene in solution are similar in shape to the ones in a polymer matrix. On the other hand, the E-PL measurements show very different results from the ones in solid films. Both monomer fluorescence and excimer fluorescence are enhanced by application of electric field in solution, contrary to the measurements of pyrene in film, in which both excimer fluorescence and monomer fluorescence are de-enhanced by an applied electric field. Based on the analysis of the E-PL spectra in terms of the Liptay model, the difference of molecular polarizability, i.e., $f^2\Delta\bar{\alpha}$, between the excimer emitting state and the ground state is evaluated to be as large as ~270±90 $Å^3$, which is more than one order of magnitude larger than the difference between the emitting state of monomer fluorescence and the ground state. The field-induced change in PL of pyrene in solution is interpreted in terms of the field effect on excitation dynamics of pyrene. It is found that the nonradiative decay process of fluorescent excimer (k_D) is decelerated by application of electric fields. The average value of field-induced change in k_D with a field strength of 0.2 $MVcm^{-1}$ is estimated to be $-(6.5 \pm 1.2) \times 10^4\ s^{-1}$. By making a comparison between E-PL results of pyrene in solution and in films, the present results may suggest that the quenching

of the fluorescent excimer state of pyrene by oxygen is de-enhanced by application of an electric field.

In chapter 5, polarized E-PL spectra of C-(n)-P (n=2-5,10,20) were obtained in solution. Both fluorescence emissions are affected by an external electric field in solution. The monomer fluorescence decreases in intensity with decreasing chain length for $3<n\leqq 20$. Based on the E-PL results, the electric dipole moment of the fluorescent exciplex is estimated to be ~19 D in any n, and the electric dipole moment of the fluorescent monomer is estimated to be ~5.5 D in n=10, 20. It is worth noting that the electric dipole moment in the fluorescent exciplex with n=1-5 is estimated to be 16-17 D based on the solvatochromism. The field-induced change in PL of C-(n)-P in solution is interpreted in terms of the field effect on photo-induced electron transfer rate. The obtained field-induced change in electron transfer rate is as follows: -6.8×10^{6} (n=2), -1.2×10^{7} (n=3), 1.3×10^{7} (n=4), 5.1×10^{6} (n=5), 2.9×10^{5} (n=10) and 1.2×10^{5} (n=20) s^{-1} with a field strength of 0.2 $MVcm^{-1}$. The D-A distance dependence of the field-induced quenching of monomer fluorescence suggests that the intramolecular charge transfer process is affected by electric fields.

Finally the author concludes that the application of an external electric field in optical spectroscopy is powerful way to investigate both molecular properties and the excitation dynamics of liquid samples. The author believes the information obtained

in these experiments can provide deep understanding of photophysical and photochemical processes of materials and allow us to design and develop new photoactive molecular devices such as solar energy conversion system.

Publications

1. **Chiang, Hung-Chu**; Iimori, Toshifumi; Onodera, Tsunenobu; Oikawa, Hidetoshi; Ohta, Nobuhiro

Gigantic Electric Dipole Moment of Organic Microcrystals Evaluated in Dispersion Liquid with Polarized Electroabsorption Spectra

J. Phys. Chem. C, **2012**, 116, 8230-8235

2. **Chiang, Hung-Chu**; Ohta, Nobuhir

External Electric Field Effect on Fluorescence Spectra of Pyrene in Solution

J. Phys. Chem. B, **2013**, 117, 3861-3866

Conference Presentation

1. **Hung-Chu Chiang**, Toshifumi Iimori, Nobuhiro Ohta

Electrophotoluminesecnce spectra of pyrene dissolved in benzene

化学系学協会北海道支部 2011 年冬季研究発表,Sapporo,**2010**/2/2

2.**Hung-Chu Chiang**, Toshifumi Iimori, Tsunenobu Onodera, Hidetoshi Oikawa,

Nobuhiro Ohta

Electroabsorption spectroscopy of DAST microcrystals in solution

Molecular Science in Sapporo, Sapporo, **2011**/09/21

3. **Hung-Chu Chiang**, Toshifumi Iimori, Nobuhiro Ohta

Electrophotoluminescence spectra of pyrene solution

化学系学協会北海道支部 2012 年冬季研究発表会, Sapporo, **2012**/01/31

4. **Hung-Chu Chiang**, Nobuhiro Ohta

Electrophotoluminescence spectra of pyrene solution

Molecular Science), Tokyo, **2012**/09/13

5. **Hung-Chu Chiang**, Toshifumi Iimori, Tsunenobu Onodera, Hidetoshi Oikawa,

Nobuhiro Ohta

Electroabsorption spectroscopy of DAST microcrystals in solution

Photochemistry,Tokyo, **2012**/09/19

6. **Hung-Chu Chiang**, Nobuhiro Ohta

Electroabsorption and electrophotoluminescence spectra of pyrene in solution

The 13th RIES-Hokudai International Symposium, **2012**/12/13

7. **Hung-Chu Chiang**, Hung-Yu Hsu, Eric Wei-Guang Diau, and Nobuhiro Ohta

Application of Stark Spectroscopy in Absorption and Photoluminescence to Optoelectronic Functional Materials

ROCNCS-JST Work shop on Nano Devices, Taiwan, **2013**/3/5

8. **Hung-Chu Chiang**, Nobuhiro Ohta

Application of Stark Spectroscopy to photochemical reactions of materials in solution

第２９回化学反応討論会,Sendai,**2013**/06/05

Acknowledgement

The author wishes to thank several people. I would also like to thank my parents for their endless love and support. Furthermore I would like to thank Dr. Takakazu Nakabayashi and Dr. Toshifumi Iimori as well for their guidance with this paper. Last but not least, I would like to thank my supervisor Nobuhiro Ohta for letting me to use this issue for my thesis.